ST. ANTHONY FALLS HYDRAULIC LABORATORY
UNIVERSITY OF MINNESOTA

Project Report No. 57

EXPERIMENTAL STUDIES OF AIR VENTILATION OF VERTICAL, SEMI-SUBMERGED BODIES

Submitted by
LORENZ G. STRAUB
Director

Prepared by
J. M. WETZEL

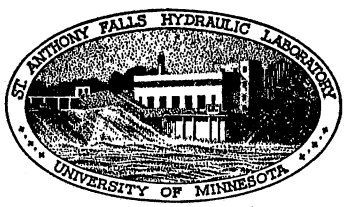

July 1957

Prepared for
OFFICE OF NAVAL RESEARCH
Department of the Navy
Washington, D.C.
Office of Naval Research Project No. NR 062-192,Contract Nonr-710(04)

PREFACE

The air ventilation of a surface-piercing hydrofoil presents a serious problem to the designer of hydrofoil craft. Several preliminary studies have been made to investigate the basic mechanism of flow ventilation and the scale-effect problem that is associated with ventilation. Previous preliminary tests at this Laboratory have indicated an absence of scale effect, but further analysis has shown that a scale effect may exist and may possibly be eliminated by consideration of secondary parameters formerly assumed to be insignificant. To extend the available knowledge in this area, fundamental studies were initiated using cylindrical rods, and later lifting surfaces in the form of streamlined vertical struts placed at an angle of yaw. The data presented for the struts should not be construed to be final, as the conclusions derived from these data may be altered as more information is obtained.

The studies covered in this report were carried out during the period December 1954 to July 1957. The project was sponsored by the Office of Naval Research under Project NR 062-192, Contract Nonr-710(04).

The entire program was under the general direction of Dr. Lorenz G. Straub, Director of the Laboratory. C. E. Bowers, as project leader was responsible for the general progress of the project as a whole. The study was conducted and the report written by J. M. Wetzel. The experimental work was performed by J. Hayek, G. Nelson, and J. Linehan.

Preparation of the manuscript for printing was carried out by Mildred McEnroe and Mary Anne Peterson under the general supervision of Loyal Johnson.

A B S T R A C T

Experimental studies were conducted to investigate the scale-effect problem associated with the ventilation of vertical, semi-submerged cylindrical rods and streamlined lifting surfaces. Several of the rods were coated with Teflon, a non-wetting material. Two types of ventilation--creeping and flash--have been observed for these shapes. Data for the large-diameter rods can be correlated with the Froude number, whereas uncoated rods of small diameter require consideration of several parameters. The use of Teflon-coated rods improved the Froude number correlation for the rods of small diameter.

Ventilation of vertical, lifting struts is primarily a function of velocity, yaw angle, submergence, and foil shape. Ventilation data of two foil shapes at high yaw angles can be correlated with the Froude number based on chord. Ventilation data at low yaw angles have not been successfully analyzed.

Some data are presented for the spanwise and chordwise pressure distributions about a surface-piercing dihedral hydrofoil (NACA 0012) at several angles of attack and dihedral angles. Distributions were obtained at subcritical and supercritical velocities. A tendency was noted for the center of pressure to move forward as the measuring section approached the free surface.

C O N T E N T S

LIST OF ILLUSTRATIONS

LIST OF SYMBOLS

c - Chord.

d - Water depth.

g - Acceleration of gravity.

h - Depth to any point on body.

w - Specific weight of fluid.

x - Distance from leading edge.

C_c - Chordwise force coefficient.

C_d - Section drag coefficient.

C_ℓ - Section lift coefficient.

C_p - Pressure coefficient.

C_L - Total lift coefficient.

C_N - Normal force coefficient.

D - Rod diameter.

H - Body submergence measured from still water surface.

L - Characteristic length.

P - Pressure at any point.

P_o - Static pressure.

V - Ventilation velocity.

V_o - Free stream velocity.

AR - Aspect ratio.

α - Geometric angle of attack (dihedral foils).

γ - Dihedral angle.

μ - Dynamic viscosity.

ν - Kinematic viscosity.

ρ - Mass density of fluid.

σ - Surface tension.

σ_i - Cavitation index.

ψ - Angle of yaw (vertical struts).

ω - Kinematic capillarity.

EXPERIMENTAL STUDIES OF AIR VENTILATION OF VERTICAL, SEMI-SUBMERGED BODIES

I. INTRODUCTION

The St. Anthony Falls Hydraulic Laboratory has entered into a contract with the Office of Naval Research to undertake fundamental studies on hydrofoils. The initial studies were directed toward obtaining information on the hydrodynamic characteristics of dihedral hydrofoils, both deeply submerged and surface-piercing. Results of the initial phase of the program have been published in Project Report No. 41 [1]*. During the course of these studies, it was observed that for certain conditions the fluid would no longer follow the upper surface of the foil but would spring free near the leading edge. Air entered the suction side of the foil and created a sudden decrease in lift. (These ventilation phenomena were also observed earlier by Benson and Land [2].) An approximate analysis was developed using the pressure momentum principle but was not completely verified by experimental data. In an attempt to arrive at a satisfactory solution to the scale-effect problem apparently associated with ventilation, additional experimental studies were initiated at the Laboratory. To obtain more information concerning the basic mechanism of flow ventilation, a limited number of pressure distributions was taken for a particular hydrofoil section and for several dihedral angles for subcritical and supercritical flow conditions. The study was curtailed at the request of the sponsor and other tests performed in a rotating-arm tank to investigate scale effects associated with ventilation of an elementary shape such as the circular cylinder; this simplified the initial work by elimination of the complex flow about a lifting surface. In this latter test it was possible to vary the fluid properties and determine their relative effect on ventilation inception. The tests in the rotating-arm tank were also extended to include vertical, streamlined struts at an angle of attack or yaw. The study is being continued currently, and some of the significant preliminary results of the tests are included in this report.

---

*Numbers in brackets refer to the Bibliography on p. 21

The report is divided into two sections, each section describing a special phase of the ventilation research: (1) Ventilation of vertical, semi-submerged circular cylinders, and (2) ventilation of vertical, semi-submerged lifting struts of streamlined shape. As the pressure distribution study was of limited scope, the data are presented in the Appendix.

II. VENTILATION OF VERTICAL, SEMI-SUBMERGED CYLINDERS

A. General Considerations

As previously indicated in the Introduction, because of the complicated shape of a hydrofoil section and the number of parameters influencing the flow about a foil, it was suggested by a representative of the sponsor that fundamental ventilation studies be conducted utilizing a simple geometric shape, such as the circular cylinder. Of primary concern was the significance of the Weber and Froude numbers on ventilation of cylinders. The effects of the Reynolds number and non-wetting agents were later investigated.

For purposes of this report, it is desirable to define the ventilation of a cylindrical rod. As the rod moves through the fluid, at a certain velocity an air pocket will form behind the rod that may or may not extend completely to the bottom of the rod. Depending on the rod diameter and submergence, two types of ventilation may be observed: (1) A "creeping" ventilation where the air pocket gradually increases in depth with increasing velocity, and (2) a "flash" ventilation where the air pocket forms very suddenly at a certain critical velocity with little or no previous depression being observed behind the rod. The first type--creeping ventilation--can be related to the Froude number based on submergence of the rod by consideration of the pressure coefficient.

Consider a vertical circular cylinder with a diameter D and submergence H moving at a velocity V_o through still water. Let h be the depth, measured from the still water surface of the air pocket behind the rod moving at the velocity V_o. When $h = H$, $V_o = V$, a critical velocity, the pocket is extended completely to the bottom of the cylinder and full ventilation takes place. If the pressure coefficient is defined as

$$C_p = \frac{P - P_o}{1/2 \rho V_o^2}$$

where P = pressure at any point

P_o = static pressure

ρ = fluid density

V_o = rod velocity

then, at ventilation

$$P - P_o = P_a - (wh + P_a) = -wh$$

where w = specific weight of the fluid. Thus, when complete ventilation occurs, the pressure coefficient becomes

$$C_p = \frac{-wH}{1/2\,\rho\,V^2} = \frac{-2gH}{V^2} = \frac{-2}{F_H^2}$$

or on an average of $-1/F_H^2$ which is dependent on the Froude number based on submergence. It was determined experimentally that it was necessary to attain a critical Froude number of approximately 1.7 before complete ventilation would occur.

The pressure coefficient is also equal to the negative of the cavitation index σ_i as commonly defined, i. e.,

$$C_p = -\sigma_i$$

As the Froude number increases, σ_i decreases, and the cavity length increases. When σ_i is above the critical value of the Froude number, complete ventilation will not be likely to occur. Flash ventilation as previously defined did not usually occur for the larger rods. To obtain flash ventilation, it was necessary to use rods with small diameters. As in the case of creeping ventilation, the basic mechanism of flow ventilation was of considerable interest as were the parameters governing ventilation of these rods, particularly with regard to scale effect. Various modeling parameters --Froude, Reynolds, and Weber--were considered in an effort to solve the problem of scale effect that is associated with ventilation. In the consideration of the importance of these parameters, two were investigated simultaneously: either the Froude and Reynolds, Froude and Weber, or Reynolds and Weber. It can be demonstrated that to investigate these parameters, some of the fluid

properties must be altered according to a specified relationship with the length ratio.

If the Froude number is defined as

$$F = \frac{V}{\sqrt{gL}}$$

where L is a characteristic length, then the condition for dynamic similarity or inertia and gravity forces is

$$\frac{V_1}{\sqrt{gL_1}} = \frac{V_2}{\sqrt{gL_2}}$$

or

$$V_r^2 = L_r$$

where L_r = length ratio
V_r = velocity ratio

The condition for constant Weber number (inertia and surface tension forces) $V\sqrt{L\rho/\sigma}$ is

$$V_1\sqrt{\frac{L_1\rho_1}{\sigma_1}} = V_2\sqrt{\frac{L_2\rho_2}{\sigma_2}}$$

or

$$V_r^2 = \frac{\sigma_r}{L_r\rho_r} = \frac{\omega_r}{L_r}$$

where σ_r = surface tension ratio
ρ_r = density ratio
ω_r = kinematic capillarity ratio

To satisfy both modeling laws simultaneously, i. e., to scale inertia, gravity, and surface tension forces, the ratio of the two numbers must be considered, as once the length ratio is determined, the velocity ratio is immediately fixed by the Froude law. Using this velocity ratio for the Weber number, it is found that

$$L_r^2 = \omega_r$$

The kinematic capillarity of the fluid must be changed according to this relationship for similarity.

By similar argument it can be shown that the ratio of Froude to Reynolds number is

$$L_r = \nu_r^{2/3}$$

and the ratio of Reynolds to Weber number is

$$L_r = \frac{\mu_r^2}{\sigma_r}$$

where ν_r and μ_r are kinematic and dynamic viscosity ratios, respectively, and σ_r is the ratio of the surface tensions.

A large number of fluids exist with different viscosities, but for convenience and ease of operation, water was used rather than oils. The water was heated by an arrangement of heating coils in the tank to produce a satisfactory change in viscosity.

It is difficult to find a number of fluids with a wide range of kinematic capillarities, and after considerable investigation, it was concluded that the most satisfactory solution was to alter the surface tension of water by addition of a suitable detergent. The unfortunate limitation of the kinematic capillarities restricts the length ratio and, thereby, the range of rod sizes that can be investigated. However, it is felt that sufficient data have been taken to determine the effect of the Weber number.

A relatively large amount of data has been published on the flow about semi-submerged cylinders of finite length. Hay [3] has done considerable work in this field. He indicated that the flow is primarily a function of the Froude and Reynolds numbers, and did not investigate the effect of Weber number. (Of primary interest was the resistance of the cylinders, rather than the velocity for occurrence of flow ventilation.) General comparisons with his work are made in the following sections of this report.

B. Experimental Procedure

1. Apparatus

The studies were conducted in a circular steel tank of 10-ft diameter and 2-ft depth. The tank was equipped with a rotating-arm mechanism as shown in Fig. 1. The rotating arm was driven by a 5-hp hydraulic motor through a Vickers transmission, with fluid at high pressure being provided by a hydraulic test stand. Such an arrangement provides a great range of velocities up to about 35 fps using an arm length of 3.5 ft, although the maximum useable velocity is restricted to about 20 fps because of excessive turbulence generated in the tank. The velocity was determined by a calibrated flowmeter on the hydraulic test stand and also by a tachometer generator driven by a gear fastened to the drive shaft of the arm mechanism. The rotating arm can be adjusted to various lengths, and the outer end is constructed to receive readily a variety of test body shapes. A cylindrical rod is shown attached to the arm in Fig. 1.

The circular, impermeable beach absorber placed around the circumference of the tank is very effective in absorbing the waves created by the moving test body. A 5-ft permeable wave filter constructed of hardware cloth has been placed in the center of the tank to further reduce wave action. These two items provide a reasonably smooth surface for the tests. The magnitude of the circulation, or swirl, created by the motion of the rod through the water was small and was neglected in these tests. A sufficient period of time elapsed between runs for the circulation and excess turbulence to be dissipated before the next test was begun.

2. Test Procedure

Cylindrical rods in a vertical position with nominal diameters from 1/32 to 2 in. were tested at various submergences. Several of the rods were covered with a coating of "Teflon" (tetrafluoroethylene resin) sprayed to a 1 mil thickness. These rods will hereafter be referred to as Teflon rods. A summary of the rod diameters and rod materials used in the tests is given in Table I. All dimensions are in inches.

All the rods had a smooth surface, and the ends were machined perpendicular to their longitudinal axis. For the Teflon-coated rods, the coating completely covered the submerged portion of the rod, including the milled

TABLE I

Steel	Brass	Lucite	Teflon
0.031	0.124	1.500	0.054
0.050	0.187	2.000	0.064
0.062	0.250		0.127
0.078	0.500		0.254
0.095	1.000		0.503
			0.753

end. Data were taken by visual observation of the complete ventilation to the bottom of the rod, and the velocity for this condition was noted. Repeat tests have indicated that this point could be observed accurately and data could be reproduced with little difficulty. Rods with nominal diameters of less than 1/4 in. were braced to reduce lateral vibrations. Most of the rods, with the exception of the Teflon rods, were tested in tap water and also in water with altered surface tension and viscosity. The surface tension was reduced by the addition of commercial detergents, such as Alconox or All. The viscosity was changed by heating the water with hot-water coils placed on the bottom of the tank. In tests requiring a change of both viscosity and surface tension, a solution of Alconox and water was heated. By varying the concentration of detergent, the surface tension could be reduced from 72 dynes per cm to about 35 dynes per cm (0.00495 to 0.0024 lb per ft). The solutions were carefully mixed, and surface tension measurements were made and checked several times during the tests by the ring method, using a Du Nouy tensiometer. By heating the water, the kinematic viscosity could be reduced to a maximum of 1/3.4 times the original kinematic viscosity before heating. Temperatures of the fluid were taken and recorded to facilitate determination of the kinematic viscosity and surface tension.

C. Discussion of Experimental Results

1. Uncoated Rods

The velocities for complete ventilation were used to compute the various modeling parameters. For example, the Froude number based on either the rod submergence, H, or the rod diameter, D, was used as a significant parameter. Data showing the relationship of the Froude number and a dimensionless submergence ratio, H/D, are plotted in Figs. 2 and 3. The broken

line is taken from results by Hay, indicating that the ventilation velocity for certain submergences and diameters can be computed with sufficient accuracy by $V/\sqrt{gH} = 1.7$.

The St. Anthony Falls data, particularly for the large rods at essentially all but the smallest submergences, appear to verify Hay's data. Data for the smaller diameter rods do not agree as well except at the large submergence ratios. The Froude number of approximately 1.7 may be regarded as a critical Froude number, as this approximate value must be approached from the decreasing side before ventilation would occur for most of the rods tested. Another interesting observation can be made from these data, with particular reference to the data plotted as a function of the Froude number based on diameter (Fig. 3). For the smaller rods, the ventilation Froude number is nearly independent of the submergence ratio, i. e., for a rod of given diameter, the velocity for complete ventilation remains essentially constant for the submergences tested. As the rod diameter increases, the same trend is observed, but over a smaller range of submergences (low submergences). For the larger rods used, this feature was not as apparent. During the tests it was observed that the ventilation of the small rods occurred in general as flash ventilation, with an increasing tendency for creeping ventilation as the diameter and submergence increased. For the large rods, no flash ventilation was observed. This is in direct agreement with the trends of the data as shown in Fig. 3. It therefore appears that a characteristic feature of flash ventilation is the independence of the submergence and ventilation velocity for a rod of given diameter. This has also been verified in conjunction with the tests of the Teflon rods as described in the following Section 2.

As the data for the different rod diameters do not reduce to a single line, it seems apparent that the Froude number does not completely define the ventilation phenomena, with the exception of those conditions where the data approach the critical Froude number of approximately 1.7, based on submergence.

The same data plotted as a function of the Reynolds number are shown in Fig. 4. For small rods of given diameter, the ventilation velocity is nearly independent of the submergence ratio, or since the diameter is constant, independent of the rod submergence itself. As the rod diameter increases, the ventilation velocity becomes more dependent on the submergence. The Reynolds number does not correlate rod ventilation data, as indicated by the different curves formed with data for each rod diameter.

To investigate the problem of scale effect, the first series of tests was made with rods of diameters from 0.35 in. to 2.0 in. and the effect of the Weber number was of primary concern. Later tests were made using rods with nominal diameters of 1/32 in. to 1/4 inch. The significance of the Weber number is shown in Figs. 5 to 9 for several rod sizes. The surface tension of the water was reduced according to the equation $L_r^2 = \omega_r$ (ratio of Froude number to the Weber number) where the length ratio was taken as the ratio of the rod diameters.

In Figs. 5, 6, and 7 three curves are shown in each of the graphs. Two of these curves are for the same rod diameter, and represent data taken in water with different surface tensions. The two curves are shown primarily to illustrate the shift of the data caused by a change in surface tension from 72 to 42 dynes per cm. If the ventilation phenomena were a function of the inertia, gravity, and surface tension forces only, then the data for the smaller rod taken in water with a surface tension of 42 dynes per cm should compare with the data for the larger rod taken in tap water with a surface tension of 72 dynes per cm. It seems apparent that the data do not verify the initial assumption completely.

In Figs. 8 and 9, only two curves are shown for the three sets of data, one for each of the rod diameters considered. The shift of the data for the smaller rod created by the change in surface tension from 67.5 to 41.9 dynes per cm in Fig. 8 or 40.9 dynes per cm in Fig. 9 is shown by different symbols, as indicated by the legend on these figures. The data for the smaller rod taken in water with a surface tension of 41.9 or 40.9 dynes per cm should compare with the data for the larger rod taken in tap water with a surface tension of 67.5 dynes per cm. It appears that for rods with diameters over 0.35 in., surface tension has little or no effect on the ventilation phenomena. However, from the previous figures for rods with diameters under 0.25 in., the Weber number has a slightly greater effect, but it still appears that other parameters or variables are of considerable significance.

The next series of tests was initiated to investigate the significance of the Reynolds number with respect to ventilation, particularly for the smaller rods. By heating the water, the viscosity was changed according to the equation $L_r = \nu_r^{2/3}$, the assumption being made that ventilation is a function of inertia, gravity, and viscous forces only. Both the Reynolds

and Froude numbers were based on rod diameter. The effect of the Reynolds number correction is shown in Figs. 10 and 11 for several rod diameters.

If for the moment attention is confined to a particular rod diameter, say 0.062 in., it can be seen that two sets of data exist for this particular diameter (Fig. 10). The solid line represents data taken in water at 17 C, whereas the broken line through the open triangles represents data taken in water at about 48 C. The comparison of these two curves illustrates the shift of the data in the proper direction with reduction of viscosity; however, the magnitude of this change is not sufficient to produce good correlation of the data for the 0.062-in. and 0.095-in. rods. The same general trend can be seen for the other rod diameters in these figures.

A group of tests was also initiated to determine the effect of the Weber and Reynolds numbers together. The tests were conducted in water in which the surface tension and viscosity were changed, thereby assuming that the ventilation was a function of both the Reynolds and Weber numbers. As previously mentioned, the viscosity was changed by heating, and the surface tension was changed by addition of a suitable detergent, in this case Alconox. This change of fluid properties was done according to the relationship $L_r = \mu r^2 / \sigma_r$, which is the ratio of the Reynolds number to the Weber number for a density ratio of unity. The results of these tests are plotted in Fig. 12. In Fig. 12(a), a comparison is made between rods of two different diameters, 0.031 in. and 0.050 inch. The solid line represents a faired line through data for the 0.050-in. rod, taken in tap water at 17 C. The open circles are data for the 0.031-in. rod tested in water with altered surface tension and viscosity. The data for the 0.031-in. rod compare very favorably with the data for the 0.050-in. rod, indicating that the assumption made was probably correct. The broken line drawn through the open triangles is data for the 0.031-in. rod, tested in water with altered viscosity, and assuming that inertia, gravity, and viscous forces predominated. The data do not follow the solid line for the 0.050-in. rod; therefore the latter assumption does not appear to be justified.

Figure 12(b) consists of data comparing an 0.050-in. rod with an 0.062-in. rod in tap water at 17 C; the faired data form the solid line. The open triangles for the 0.050-in. rod assume the Weber-Reynolds relationship is correct, whereas the open circles assume the Reynolds-Froude relationship

is correct. It appears that the Weber-Reynolds assumption gives slightly better results, as the triangles plot closer to the solid line than do the circles.

Larger rods, 0.062-in. and 0.095-in., are compared in Fig. 12(c). The solid line represents data for the 0.095-in. diameter rod in tap water. The 0.062-in. rod was tested in water with reduced viscosity and surface tension following the Weber-Reynolds assumption, and the data are shown by the triangles. The data do not agree as favorably as for the smaller rods; however, it appears to be better than the data assuming a Froude-Reynolds relationship, as shown by the open circles, particularly for the lower submergence ratios.

Figure 12(d) shows a comparison of data for the 0.062-in. rod and the 0.124-in. rod, data for the latter being shown by the solid line. The data shown by open and solid symbols were again taken in water with reduced viscosity and surface tension, assuming the Weber-Reynolds relationship to hold. The data do not fall on the solid line for the 0.124-in. rod; therefore, the assumption made is probably not correct. Other parameters may considerably influence the ventilation phenomena for these rod diameters. The open symbols represent data taken for a specified viscosity and surface tension, as given by $L_r = \mu r^2 / \sigma_r$. The solid symbols represent data taken for the same rod in water with a different combination of viscosity and surface tension; however, the ratio as indicated above remains essentially the same. The data agree favorably in both cases.

The data plotted in Fig. 13 are for a 0.562-in. rod and a 0.75-in. rod, assuming inertia, gravity, and viscous forces predominate. The two graphs show the same data plotted against the Froude number and the Reynolds number. In the plot for the Froude number, the solid line represents data for the 0.75-in. diameter rod in tap water at 25.5 C. The open symbols represent data for the 0.562-in. diameter rod in tap water at 50 C, the viscosity thereby being reduced. The agreement for the two different rods is very good, indicating that the assumption was probably correct. The same data has been plotted against the Reynolds number in the second graph. For comparison purposes, two sets of data are shown for the 0.562-in. rod for different water temperatures and viscosities. The open symbols show data for the 0.562-in. rod at 50 C, and compare favorably with the 0.75-in. rod at 25.5 C. The data for the 0.562-in. rod have experienced a considerable shift with a decrease in

viscosity. It appears that although fair definition of the ventilation phenomena of the larger rods is achieved by consideration of the Froude number alone, as can be seen from Fig. 2 or 3, the Reynolds number correction will improve this definition, particularly for the lower submergence ratios.

From these plots, it seems apparent that as the data for several rod sizes fall on a single curve, the Weber-Reynolds laws give satisfactory results for the smaller rods, with the agreement becoming poorer as the rod diameter increases. It thus appears that a certain range of diameters and submergence ratios exists where all three numbers---Reynolds, Weber, and Froude---have a significant effect on ventilation. In an attempt to reduce the effect of surface tension, several rods were coated with a non-wetting material. The results of these studies are given in the following section.

2. Teflon Rods

Plots of faired curves of the data for the submergence ratio H/D against the Froude numbers are shown in Fig. 14 for the six Teflon rods used in this study. The broken line in Fig. 14(a) is again based on extrapolation of Hay's data. The St. Anthony Falls data indicate that a Froude number based on submergence of approximately 1.7 must be exceeded before complete ventilation would occur. This is true especially for the larger rods, or for the smaller rods at the higher submergence ratios. As the ventilation velocities extrapolated from Hay's data are dependent on the submergence for a rod of given diameter, the data are apparently for creeping ventilation. Figure 14(b) is a plot of the St. Anthony Falls data for the submergence ratio against the Froude number based on diameter. The ventilation velocity varies with submergence for a particular rod diameter, indicating that creeping ventilation is predominant. This was also verified by observation during the tests. The data for rod diameters larger than 0.254 in. essentially fall on the same line for most submergence ratios, indicating that the Froude number is the proper modeling parameter for these particular submergence ratios and diameters.

Figure 15 shows a comparison of the data for the Teflon rods and steel rods as a function of the submergence ratio and the Froude numbers based on both submergence and rod diameter. The solid line in each of the plots is a faired line through the data for the Teflon rods, whereas the broken line is a faired line through data for the steel rods. (To avoid confusion in the case of large rod diameters, the steel rod data are represented by circles.)

It seems clear that a marked difference in ventilation velocity exists between a small steel rod and a Teflon rod of the same diameter and submergence. This difference diminishes in magnitude as the rod diameter increases or the submergence ratio increases. For rods larger than 0.254-in. diameter, the ventilation of the steel rod and Teflon rod behaves in the same manner. The large difference of ventilation velocity between the small steel rods and Teflon rods is indicative of the difference between creeping and flash ventilation. In general, the small steel rods ventilate suddenly--flash--whereas the Teflon rods ventilate gradually--creeping. For the larger rods, ventilation occurs as creeping ventilation for both rod materials.

In some cases, it was possible to obtain creeping ventilation for the small steel rods. However, this was rather unusual as the occurrence of flash ventilation greatly predominated. In Figs. 16 and 17, the data for the Teflon rod and for both types of ventilation for the steel rod are plotted. The open circles represent data for the steel rod and the solid circles represent data for the Teflon rod. It is interesting to note that the data for the creeping ventilation of the steel rod and the Teflon rod agree very favorably for the rods tested. (Data for rods above 0.25-in. diameter are not shown, as creeping ventilation occurred for both cases, and the data agree as indicated in Fig. 15.)

During the course of the tests, data were also taken for the closing or disappearance of the vent. These data give an indication to the hysteresis effect associated with the rod ventilation phenomena. Figures 18 and 19 show this effect for the four smaller rods. The data for the Teflon rods are shown in open symbols, and the data for the steel rods in crossed-open symbols. Several ventilation conditions are noted on these plots. Considering first a Teflon rod of given diameter and submergence, the open triangle represents the velocity at which ventilation first appears. The velocity is gradually increased until the ventilation is complete to the bottom of the rod (circles). As the velocity is gradually decreased, the ventilated pocket behind the rod also decreases in magnitude, until finally a velocity is reached where the pocket disappears completely. This point is shown by the open squares. In the case of the Teflon rods tested (and therefore creeping ventilation), it appears that little hysteresis effect is found, as the vent disappears at approximately the same velocity at which it appeared. This result is slightly more noticeable for some diameters than for others, but the general trend appears to be the same in all cases.

For the steel rods (flash ventilation) a very marked hysteresis was observed. Air entered suddenly to the bottom of the rod, with little or no previous indication of a depression forming behind the rod. As a result, only the velocity for complete ventilation could be determined, and this was considerably higher than the velocity for complete creeping ventilation. As the velocity was reduced, a certain velocity was reached where the vent would disappear and this point is shown by the crossed circles on Figs. 18 and 19. These data agree essentially with the data obtained for the vent disappearance for the Teflon rods. In several instances it was possible to obtain creeping ventilation for the small steel rods, and in these cases the closing velocity was essentially the same as for the flash ventilation. Thus it seems apparent that a large hysteresis effect is found for the small steel rods, whereas little effect is found for the Teflon rods.

Figure 20 was prepared to summarize the data for the steel and Teflon rods and further demonstrate the conditions under which various modeling parameters are applicable. The solid curved lines for the steel and Teflon rods were obtained from cross-plotting the faired curves of Figs. 2 and 14(a), allowing an arbitrarily assumed error of 10 per cent in the ventilation velocity. That is, a Froude number of 1.87 was assumed in Figs. 2 and 14(a) and the intersection of this line and the curve for a specified rod diameter determined a value of H/D. The submergence H was computed for the given diameter and plotted in Fig. 20. If a smaller error in velocity is desired, another curve can be drawn on Fig. 20 that will be displaced slightly upward. Although, as previously indicated, the Froude number appears to satisfactorily correlate ventilation data of the larger diameter rods for most submergences, better correlation can be obtained by considering the Reynolds number effect for the small submergences.

The effect of a non-wetting material is evident from Fig. 20. The region for which the Froude number is applicable is further extended, as the curve is displaced below the curve for the steel rods. Apparently the non-wetting material reduces the effect of surface tension on ventilation, thereby increasing the significance of the gravity forces.

III. VENTILATION OF VERTICAL, SEMI-SUBMERGED STREAMLINED STRUTS

A. General Considerations

Of more practical interest is the ventilation of actual hydrofoil shapes operating under the influence of a free water surface. As the flow pattern about a foil becomes complex under these conditions, a vertical strut placed at an angle of attack or yaw was used initially for simplicity. If the strut is placed in the water at a certain angle of yaw and submergence, ventilation usually can be obtained by increasing the velocity of the strut moving through still water [Fig. 21(a)]. Two more or less distinct types of ventilation have been observed for the streamlined shapes. For the high yaw angles, as the velocity is increased to a certain value (dependent on foil shape, submergence and yaw angle) a pocket opens on the suction side but does not extend completely to the bottom of the strut. A relatively large amount of white water is present in the lower portion of the pocket. As the velocity is further increased, the pocket will eventually extend to the bottom of the strut and full ventilation is attained [Fig. 21(b)].

For the low yaw angles, the suction side pocket does not form gradually but opens suddenly, very similar to flash ventilation which occurs with the small diameter steel rods. The water separates completely from the leading edge of the foil and does not re-attach itself onto the foil at any point.

The two types of ventilation are separated by a small region of instability, where either type of ventilation may occur. For the larger submergences, this region is fairly well defined, and the angle of yaw for this point may for convenience be called the critical angle. It is more difficult to assign a critical yaw angle for the small submergences, but an approximate value may be used.

Some recent work by the NACA [4] on flat plates operating under the influence of a free surface agrees favorably with the results of this Laboratory, particularly with regard to correlation parameters for the high angle ventilation. The NACA data indicate correlation of low angle ventilation with a speed parameter (velocity divided by square root of foil thickness ratio). The preliminary data taken here for the lower yaw angles do not follow such a relationship, and more work must be done to support completely any definite conclusions regarding this region of ventilation.

Other interesting work on strut ventilation has been done at the California Institute of Technology [5]. The primary objectives of the study were to determine the effect of the free water surface on the apparent aspect ratio of the vertical strut, and the effect of air ventilation on the lift (cross-force) developed by the vertical foil. The foil used was a 17.5 per cent thick, symmetrical, lenticular airfoil. To investigate the effect of the free surface, the foil was attached to a reflection plane on the surface. To account for the image of the foil above the reflection plane, the aspect ratio was defined as twice the foil submergence divided by the chord. The effect of the aspect ratio on the slope of the lift coefficient curve is shown in Fig. 22(a) for several aspect ratios. Comparing results of these tests to those without a reflection plane, it was found that the effective aspect ratio of a surface-piercing strut should be taken as being equal to its geometric value.

Figure 22(b) indicates the effect of the presence of a free surface upon the lift coefficient for wetted and ventilated flow. It is interesting to note that the onset of ventilation, as indicated by the broken lines, occurs near the stall angle for this particular section. In fact, ventilation was obtained only after the stall point of the foil was reached. Studies conducted at this Laboratory with different foil sections have also qualitatively indicated agreement with this point. A considerable hysteresis effect is also associated with ventilation. Once ventilation is established, a relatively large reduction in yaw angle is necessary to obtain again a fully wetted flow for the same velocity. The sudden decrease in lift becomes apparent after the inception of full ventilation, and emphasizes the reason for avoiding full ventilation if at all possible.

The results of the California tests also indicated that a scale effect appears to exist for ventilated flows, and it may be related to surface tension or viscous effects. Surface tension effects on ventilation have been described in another California paper [6]. It was observed that the strut could operate either with or without ventilation for a certain set of conditions. If the velocity were high enough for ventilation to occur normally but it had not developed, ventilation could be initiated by turbulence or wave action on the surface as ventilation is more likely to occur when the water surface is rough, and is most likely to be suppressed in smooth water. Surface tension was considered to be a significant parameter as it prevented

air from entering the wake behind the strut, especially on small models. Further work on the scale-effect problem is being continued at the St. Anthony Falls Laboratory.

B. Test Apparatus and Procedure

The struts used in the ventilation studies were of NACA 0012 and NACA 0024 profile. Two- and 3-in. chord struts were available for the NACA 0012 section, and a 2-in. chord for the NACA 0024 section. The foils were made of brass or aluminum with a special milling cutter, hand-finished and polished. The strut was fastened to a special mounting bracket that was attached to the end of the rotating arm. The mounting bracket was constructed to readily permit adjustment of the yaw angle (to within 1/2 degree) and submergence. The majority of the tests were run in the rotating-arm tank previously described in Section II B.

A submergence and yaw angle were set for a particular foil and the velocity increased in small increments until complete ventilation was attained. The occurrence of complete ventilation was determined visually, and little difficulty was experienced in determining this condition. Attempts were made to obtain the data with a minimum of turbulence being present in the tank, which necessitated waiting for a short period of time between successive runs. A brief series of spot checks was made with the towing carriage to verify the data in the rotating-arm tank. Results are given in the following section.

C. Discussion of Experimental Results

The basic data that have been obtained are the velocity for complete ventilation for a particular submergence and yaw angle. These data are shown for the two sections in Figs. 23 and 24 for various submergence ratios. Figure 23(a) indicates the effect of small submergence ratio (1/2 to 2) on the ventilation velocity for a particular yaw angle. It is interesting to note the change in the curves with increasing submergence. For small submergences, the ventilation velocity depends largely upon the yaw angle. As the submergence increases over a certain range of yaw angles the ventilation velocity is essentially constant. A rather sharp break in the curve is noted, and the ventilation velocity then increases very rapidly for a small change in yaw angle. This trend is even more evident in Fig. 23(b) for submergence ratios of 2 to 5. The rather sharp break in the curve occurs over a relatively small

range of yaw angle, and this region may be called the critical angle. It appears that as the submergence increases the region becomes narrower, and a more definite critical angle may be assigned. For yaw angles below this so-called critical angle, ventilation was difficult to obtain. In fact, for the NACA 0012 section, if the angle were less than about 21 degrees the strut would not ventilate at the velocities available in the rotating-arm facility under normal conditions of turbulence. In general, as the turbulence level of the water in the tank increased, ventilation could be obtained at lower angles than indicated, but in this case it appeared that waves on the surface or some other external disturbance triggered the ventilation. The dotted line in Fig. 23(b) for H/C = 2 indicates the typical effect of increased tank turbulence or surface conditions. These data were obtained by letting the strut pass through disturbed water until the strut ventilated. The velocities indicated are the minimum velocities for which the foil would ventilate under these conditions.

The data apparently fall into a systematic pattern with regard to submergence, with the exception of the very small submergence ratios, such as 1/2 and 1, where surface effects become very significant.

Figure 24 is a plot of data for the NACA 0024 section. The same general features are exhibited with this foil, which is twice as thick as the NACA 0012. The greatest difference is that the curves are shifted downward. The critical angle is smaller than for the thinner section. The effect of thickness of the foil is to reduce the critical angle and increase the region for which ventilation velocity is relatively independent of the yaw angle.

Preliminary analysis has been directed toward correlating data for the sections utilized. Attempts at correlating data over the entire range of yaw angles have not been successful, but better results have been obtained by dividing the ventilation into two types: high- and low-angle ventilation, which are separated by the critical angle for the sections. The high-angle ventilation is essentially independent of yaw angle and can be correlated by the Froude number based either on submergence or chord and the submergence ratio or depth in chords. This correlation is shown in Fig. 25 for the NACA 0012 and NACA 0024 sections and for two chord sizes. In Fig. 25(a), note that the data for three foils tend to group together for the higher submergence ratios. The data are grouped about a Froude number based on submergence

of about 1.6. It is interesting to note that this value is approximately the same as for the large-diameter, circular rods (Fig. 2). In other words, the factors influencing high-angle ventilation and rod ventilation are very much the same. It also appears that foil thickness has little effect when the data are plotted in this manner.

The same basic data plotted as a function of Froude number based on chord are shown in Fig. 25(b). Again correlation of the data for the three foils is reasonably good, except at the smaller submergences. The trend of the data bears a striking resemblance to that for the circular rods (Fig. 3) plotted on the same basis, except that the strut chord replaces the rod diameter as a characteristic length.

Data for angles below the critical have not been completely analyzed at the present time and future work is being directed toward that end.

To investigate the validity of the data taken in the rotating-arm tank, several check tests were made with the towing carriage for the NACA 0012 section. Two submergence ratios were used--2 and 4--and a comparison of the data taken in the two facilities is shown in Fig. 26. The agreement is reasonably good for these sections, particularly for the higher angles of yaw and smaller submergences. A discrepancy exists in data for the larger submergence and for lower angles of yaw. This may be attributed to the fact that the disturbance in the rotating-arm tank caused by the foil was rather large at this submergence. In an effort to reduce the effect of turbulence on ventilation, in some instances it was required that the foil ventilate after perhaps only one or two complete turns. This may not have been sufficient for normal ventilation conditions to develop, and the resulting ventilation velocity would then be higher. Even for some cases in the towing facility, ventilation occurred near the very end of the test run. Disregarding this exception, it is felt that the data taken in the rotating-arm facility represent the actual ventilation phenomena as would occur in straight line motion.

IV. CONCLUSIONS

Based on the tests described in the preceding sections of this report, it is possible to derive the following conclusions:

1. Two distinct types of ventilation occur--creeping or flash ventilation. The predominating type is deter-

mined by body size, submergence, and, where applicable, angle of yaw.

2. Ventilation occurs as creeping ventilation for large-diameter uncoated rods and also for Teflon-coated rods. Flash ventilation predominates for the small, uncoated metallic rods at all but very large submergences.

3. Creeping ventilation data for the rods can be correlated with the Froude number and submergence ratio. In general, flash ventilation correlation necessitates consideration of viscosity and surface tension.

4. Little hysteresis effect exists for creeping ventilation (large-diameter rods and Teflon rods). The velocity for appearance and disappearance of the ventilated pocket is essentially the same. A very pronounced effect is found for flash ventilation (small-diameter rods).

5. The two distinct types of ventilation that occur for vertical, streamlined struts are dependent on the angle of yaw. Above a certain critical yaw angle, ventilation is primarily a function of submergence and body shape, and the ventilation velocity is essentially independent of the yaw angle. Below the critical angle, the ventilation velocity becomes increasingly dependent on yaw angle, and less dependent on submergence.

6. High-angle ventilation data can be successfully correlated with the Froude number and submergence ratio. Satisfactory correlation of low angle data has not been obtained.

B I B L I O G R A P H Y

[1] Tinney, E. Roy Experimental and Analytical Studies of Dihedral Hydrofoils. University of Minnesota St. Anthony Falls Hydraulic Laboratory Project Report No. 41, November 1954. 92 pages.

[2] Benson, J. M. and Land, N. S. An Investigation of Hydrofoils in the NACA Tank. I - Effect of Dihedral and Depth of Submersion. National Advisory Committee for Aeronautics Wartime Report L - 758. September 1942. 12 pages.

[3] Hay, A. Donald Flow About Semi-Submerged Cylinders of Finite Length. Princeton University. October 1947. 174 pages.

[4] Ramsen, John A. An Experimental Hydrodynamic Investigation of the Inception of Vortex Ventilation. National Advisory Committee for Aeronautics Technical Note 3903. April 1957. 31 pages.

[5] Kiceniuk, Taras. A Preliminary Experimental Study of Vertical Hydrofoils of Low Aspect Ratio Piercing a Water Surface. California Institute of Technology, Hydrodynamics Laboratory Report No. E-55.2. December 1954. 17 pages.

[6] Perry, Byrne Experiments on Struts Piercing the Water Surface. California Institute of Technology, Hydrodynamics Laboratory Report No. E-55.1. December 1954. 27 pages.

F I G U R E S

(1 through 26)

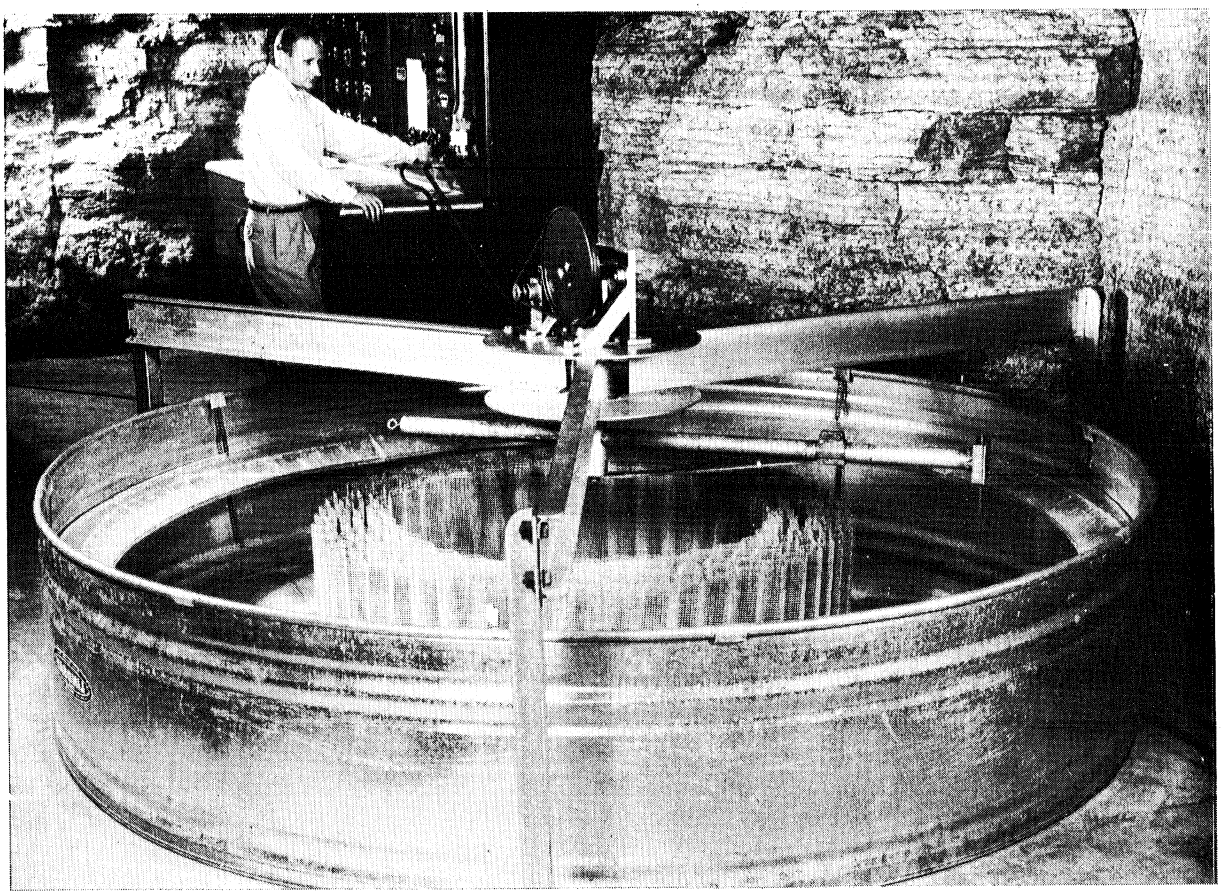

Fig. 1 - Photograph of Rotating-Arm Tank

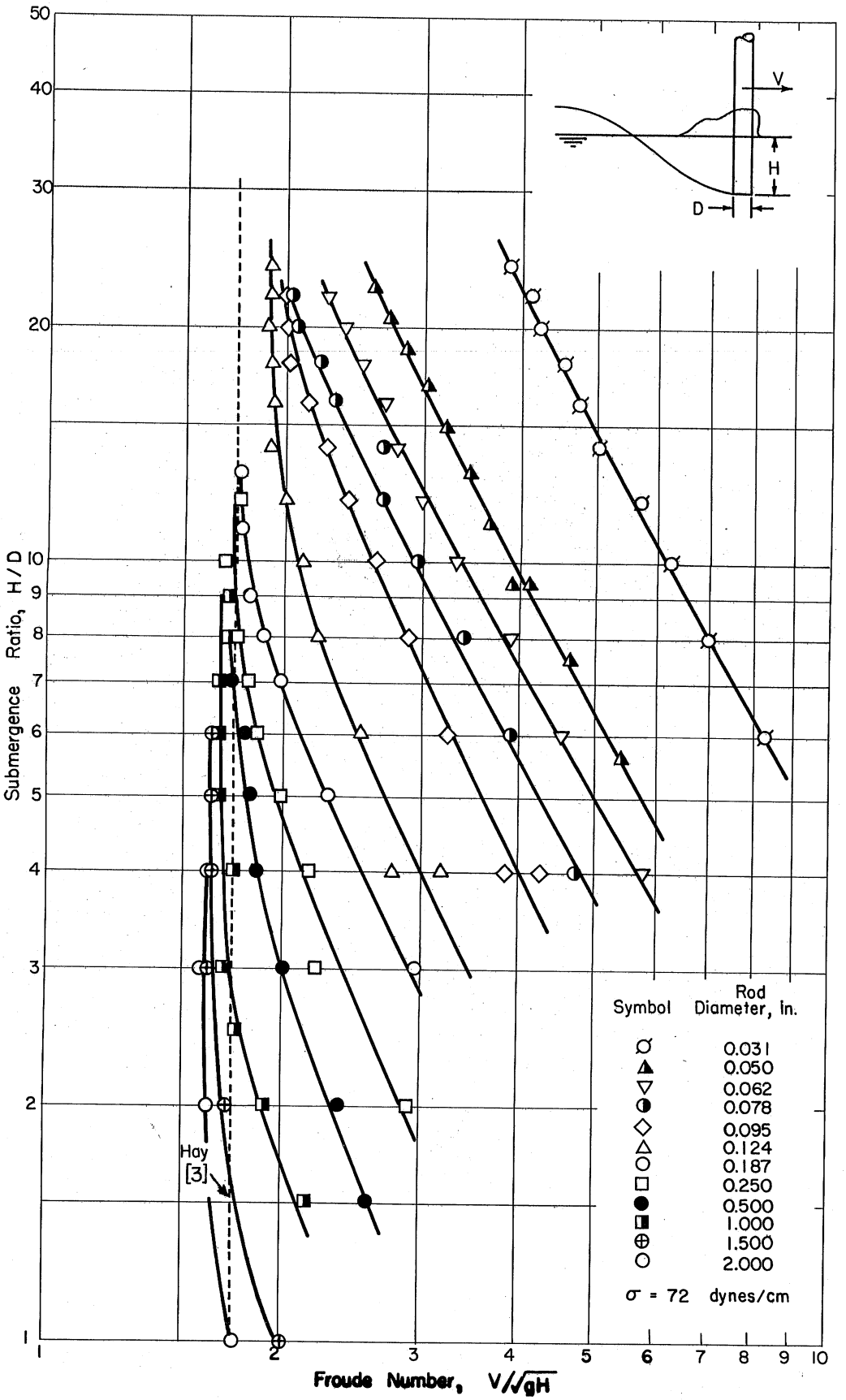

Fig. 2 – Rod Ventilation as Function of Froude Number Based on Submergence

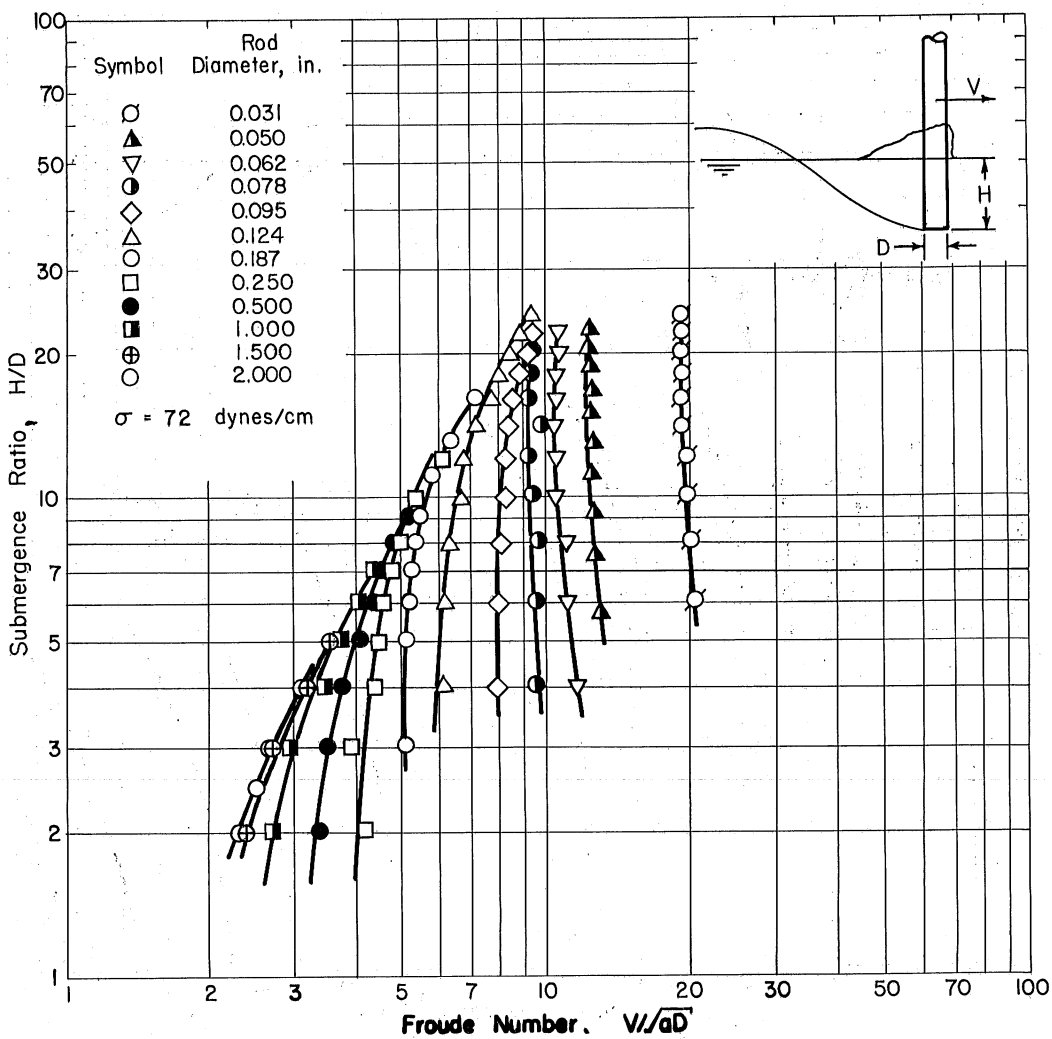

Fig. 3 – Rod Ventilation as Function of Froude Number Based on Diameter

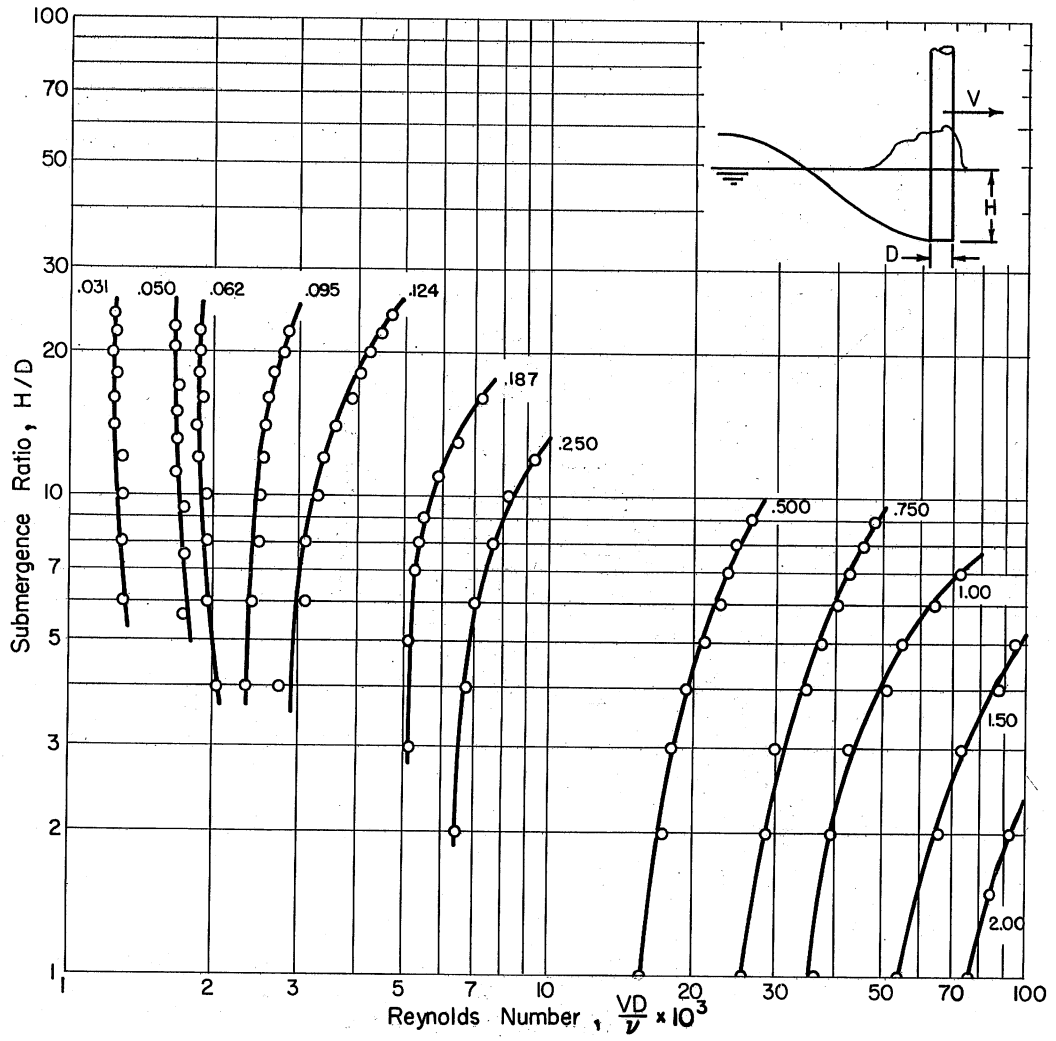

Fig. 4 – Rod **Ventilation as Function of Reynolds Number Based** on Diameter

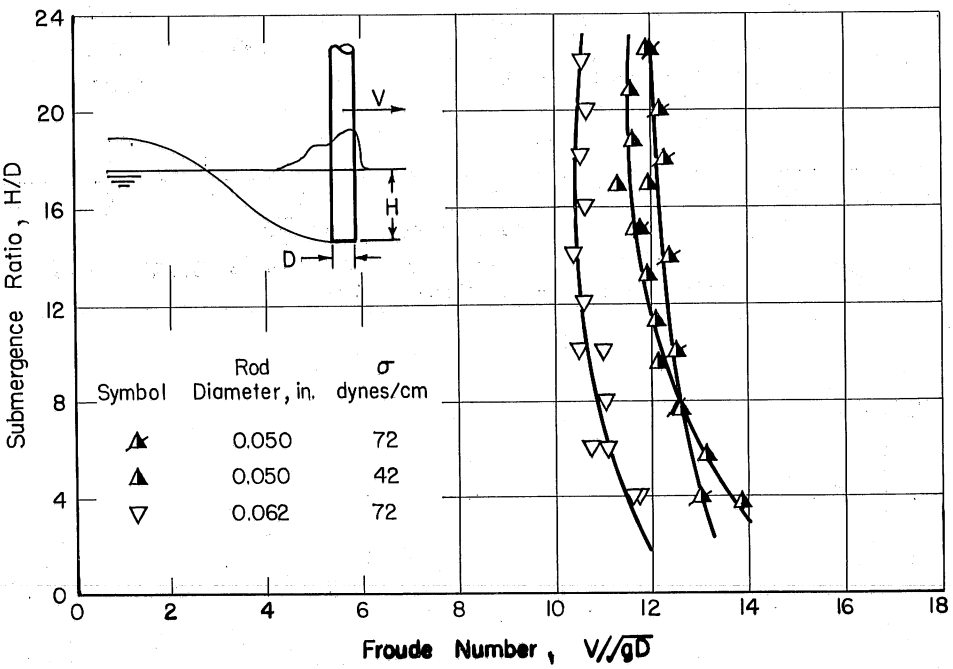

Fig. 5 - Effect of Constant Froude-Weber Ratio on Rod Ventilation (0.05-in. and 0.062-in. diameter rods)

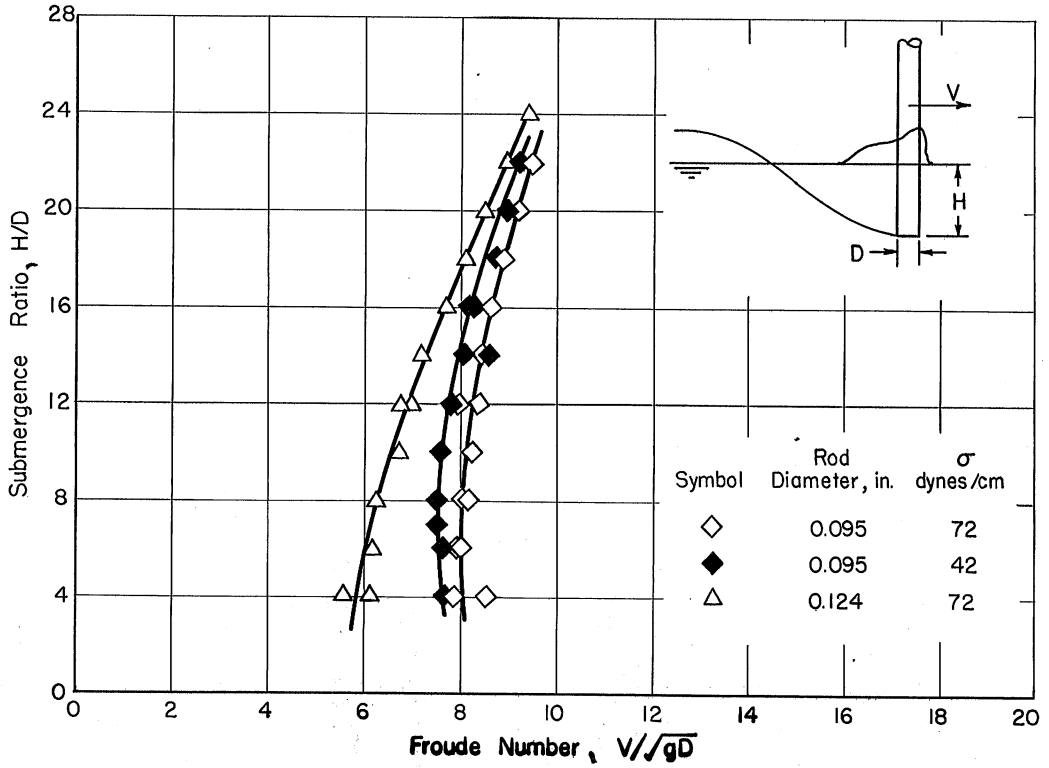

Fig. 6 - Effect of Constant Froude-Weber Ratio on Rod Ventilation (0.095-in. and 0.124-in. diameter rods)

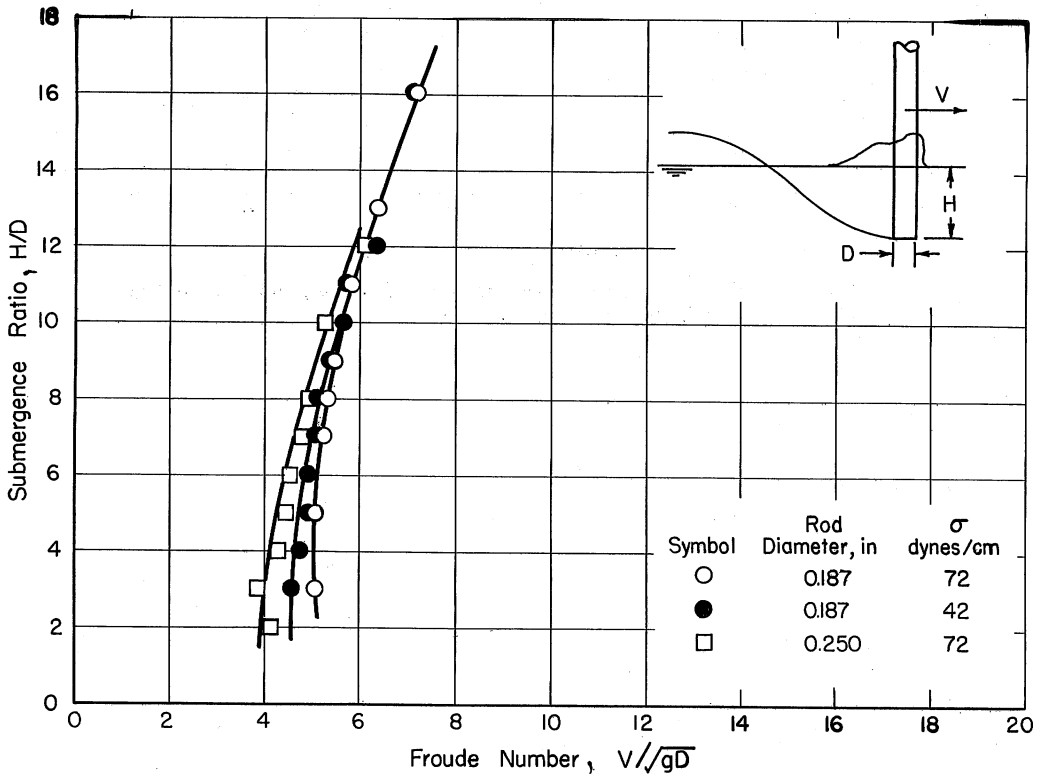

Fig. 7 - Effect of Constant Froude-Weber Ratio on Rod Ventilation (0.187-in. and 0.25-in. diameter rods)

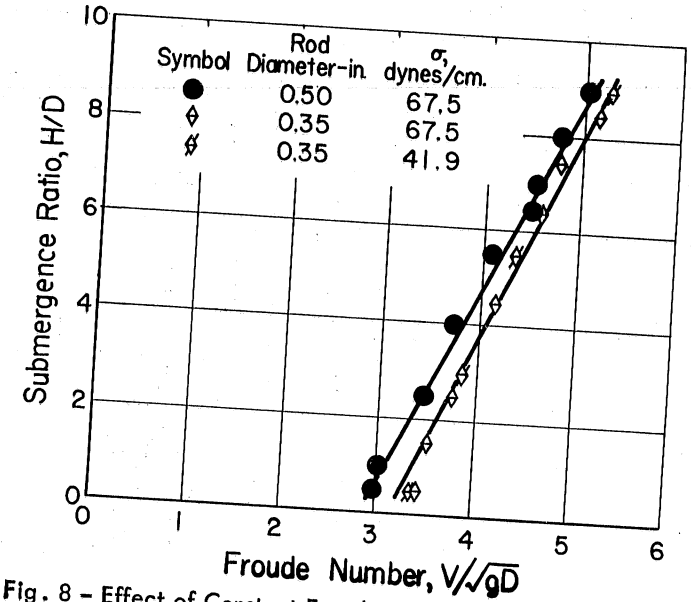

Fig. 8 – Effect of Constant Froude-Weber Ratio on Rod Ventilation (0.35-in. and 0.50-in. diameter rods)

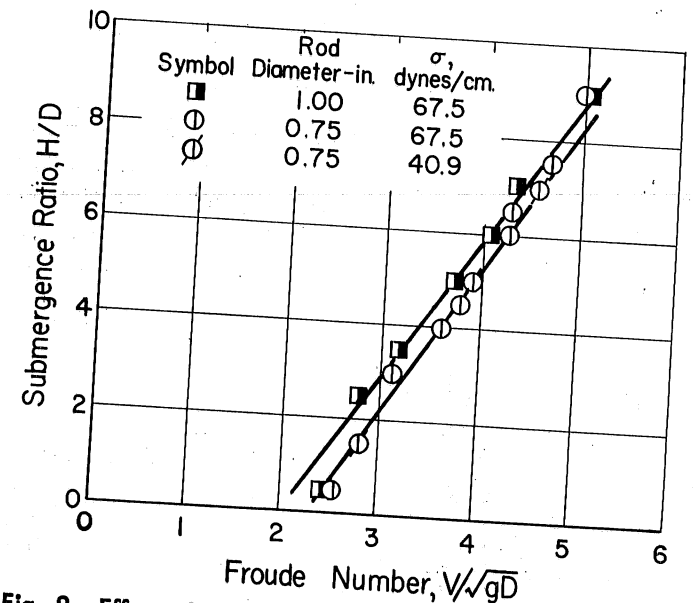

Fig. 9 – Effect of Constant Froude-Weber Ratio on Rod Ventilation (0.75-in. and 1.00-in. diameter rods)

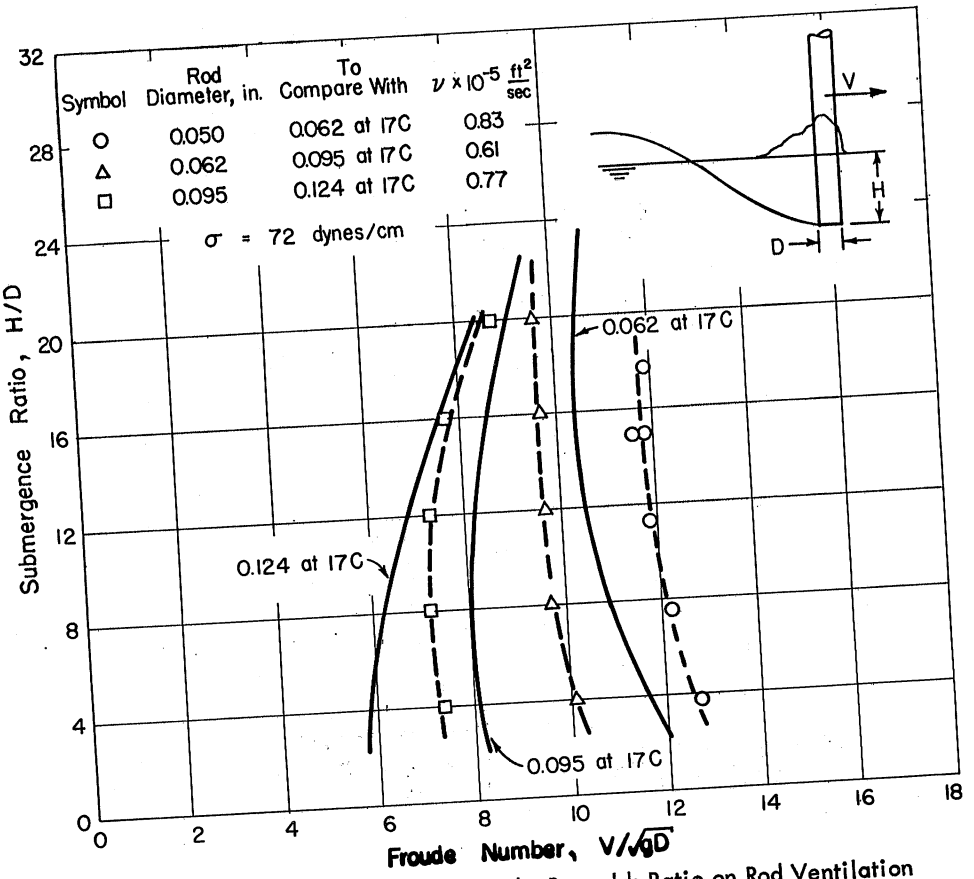

Fig. 10 - Effect of Constant Froude-Reynolds Ratio on Rod Ventilation (0.05-, 0.062-, 0.095-, and 0.124-in. diameter rods)

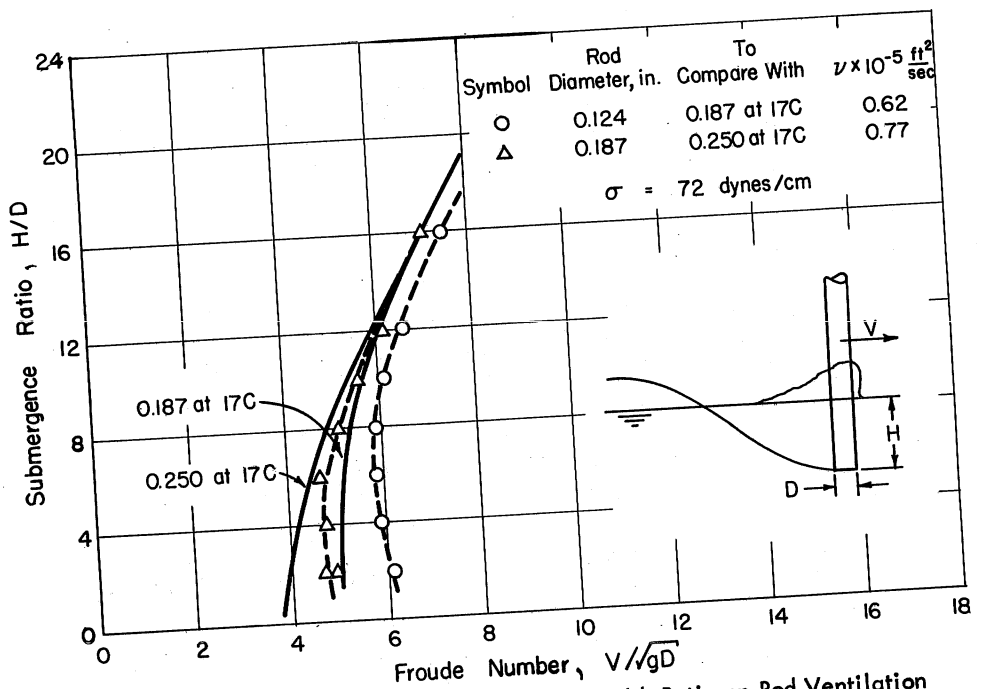

Fig. 11 - Effect of Constant Froude-Reynolds Ratio on Rod Ventilation (0.124-, 0.187-, and 0.25-in. diameter rods)

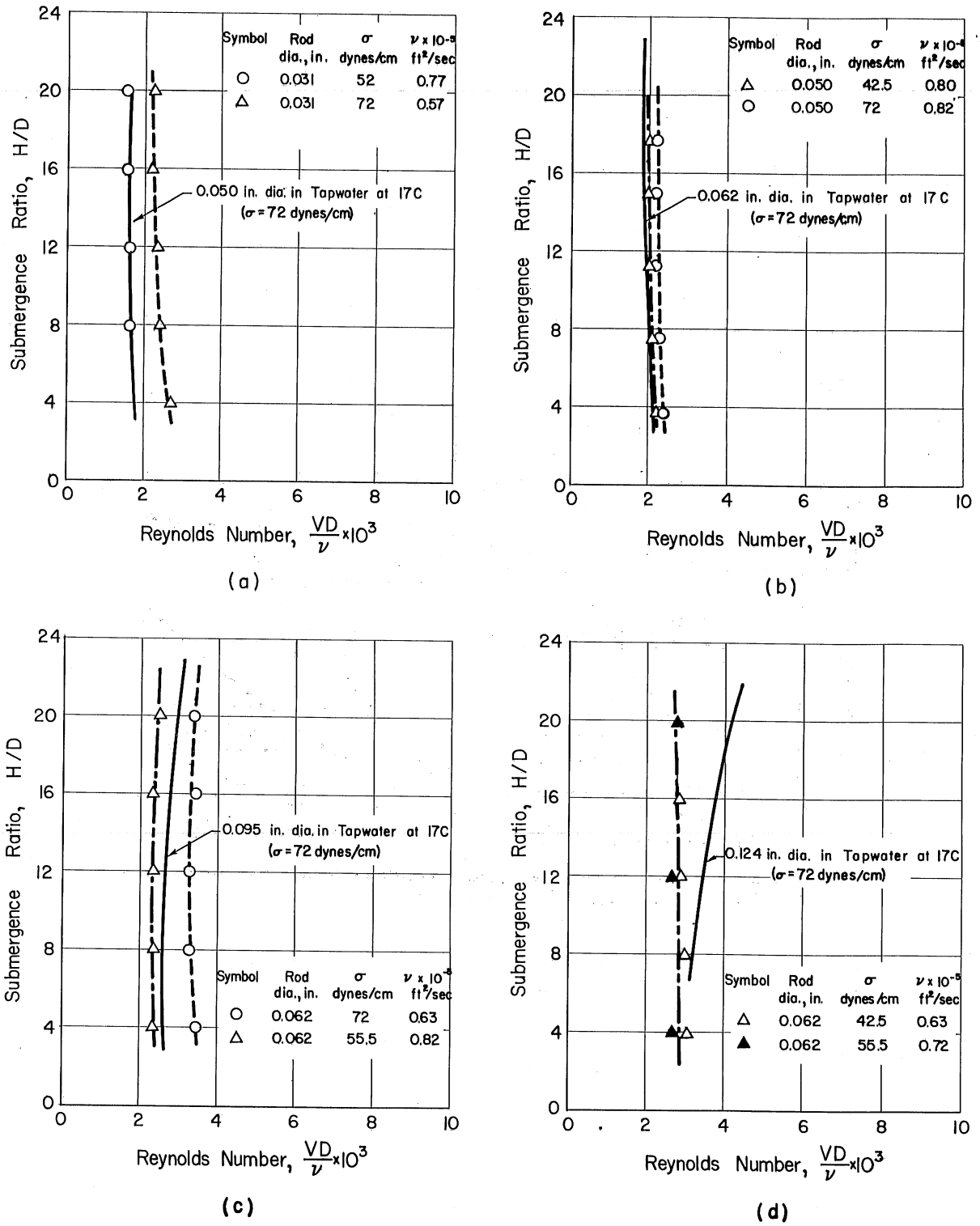

Fig. 12 - Effect of Constant Reynolds-Weber Ratio on Rod Ventilation (0.031-, 0.050-, 0.062-, and 0.095-in. diameter rods)

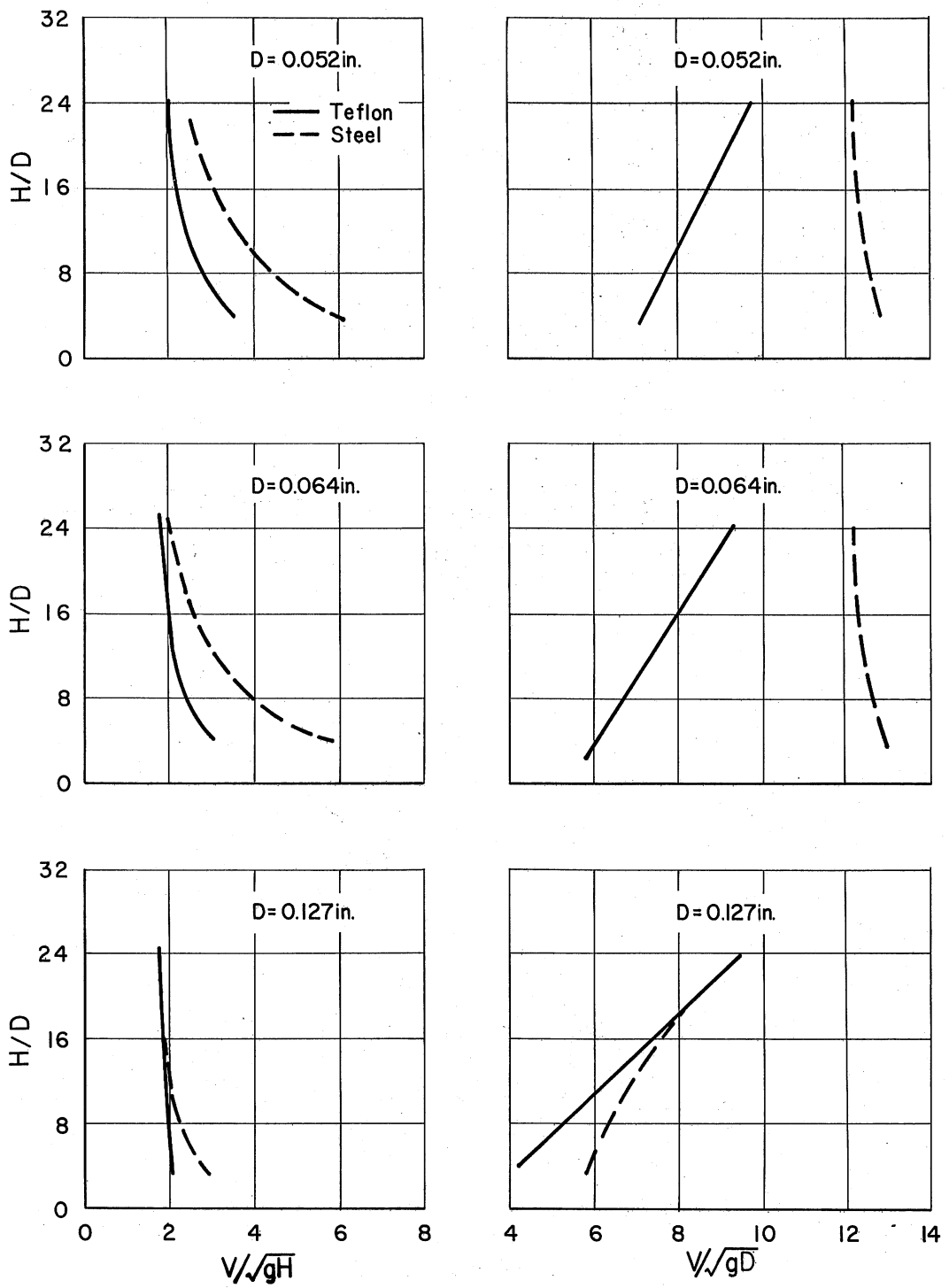

Fig. 15 - Comparison of Ventilation of Teflon and Steel Rods

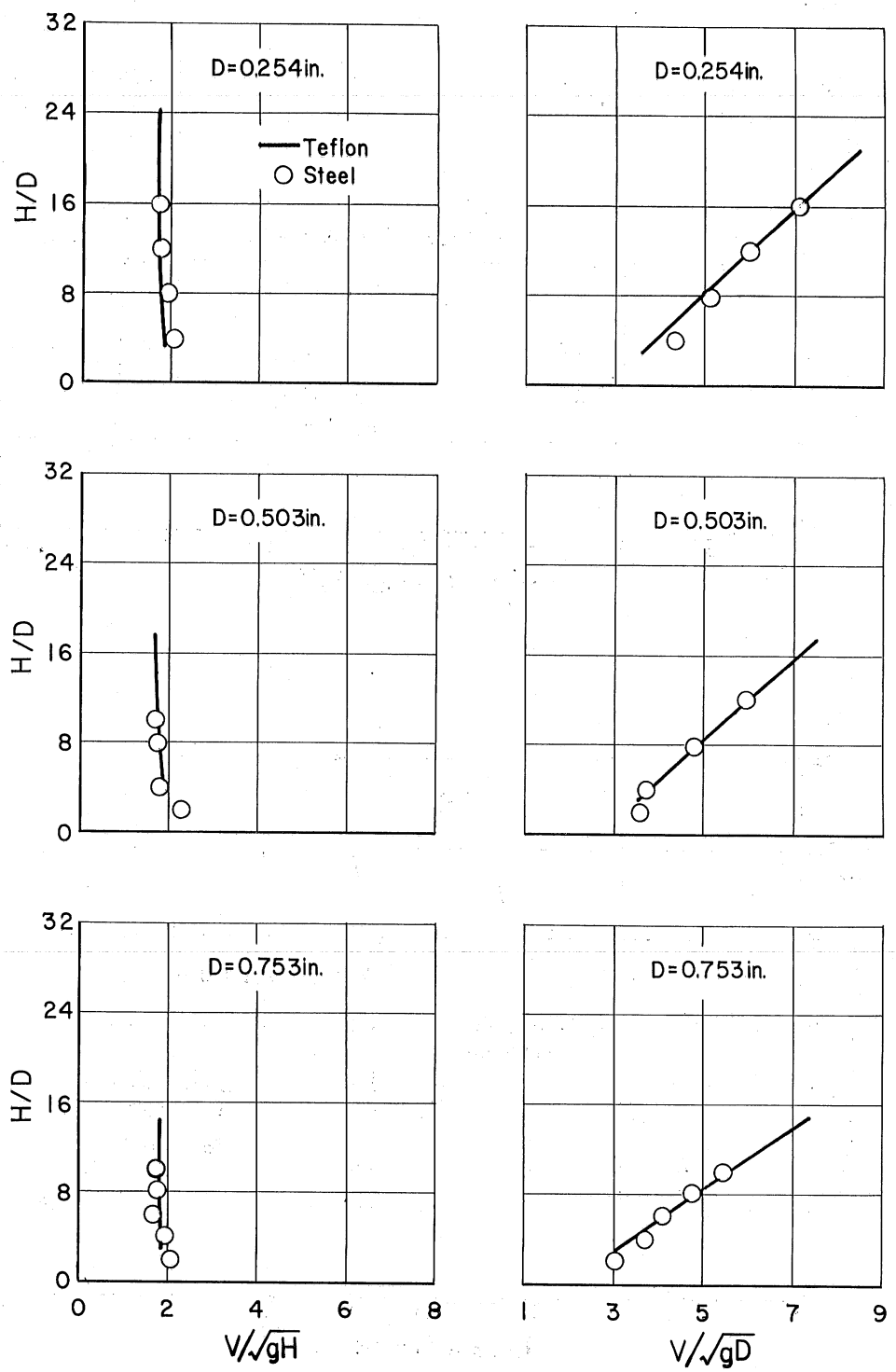

Fig. 15 (continued) – Comparison of Ventilation of Teflon and Steel Rods

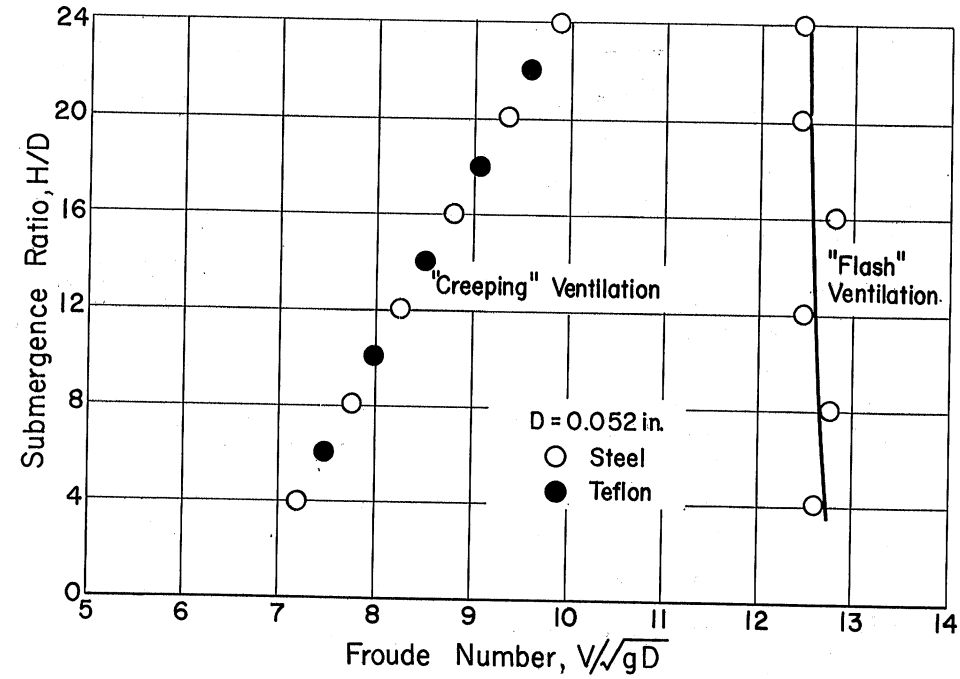

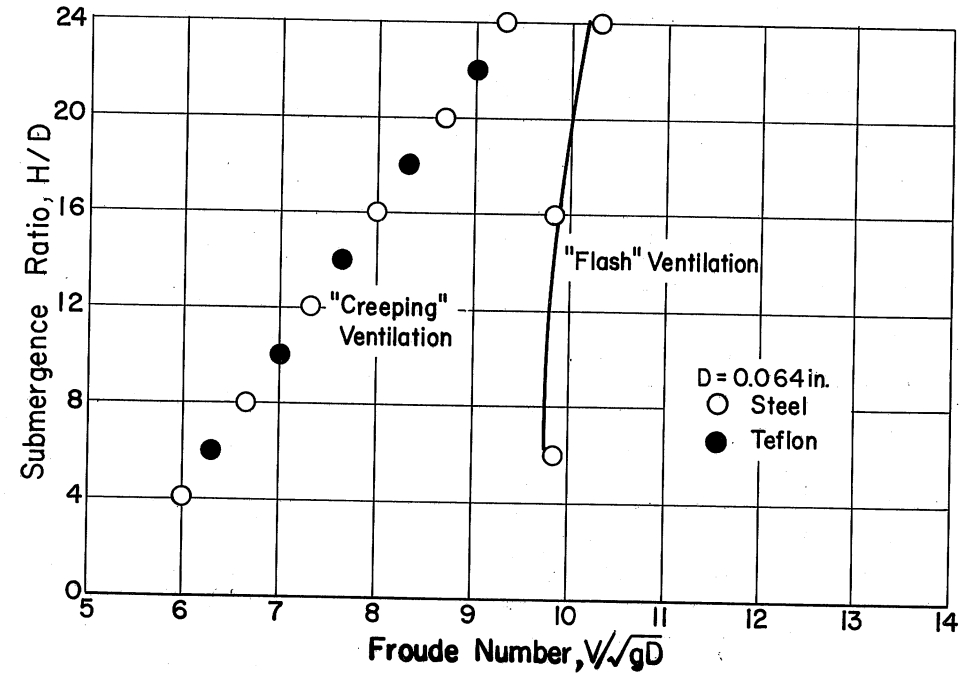

Fig. 16 – Comparison of Creeping and Flash Ventilation Froude Numbers (D = 0.052 and 0.064 in.)

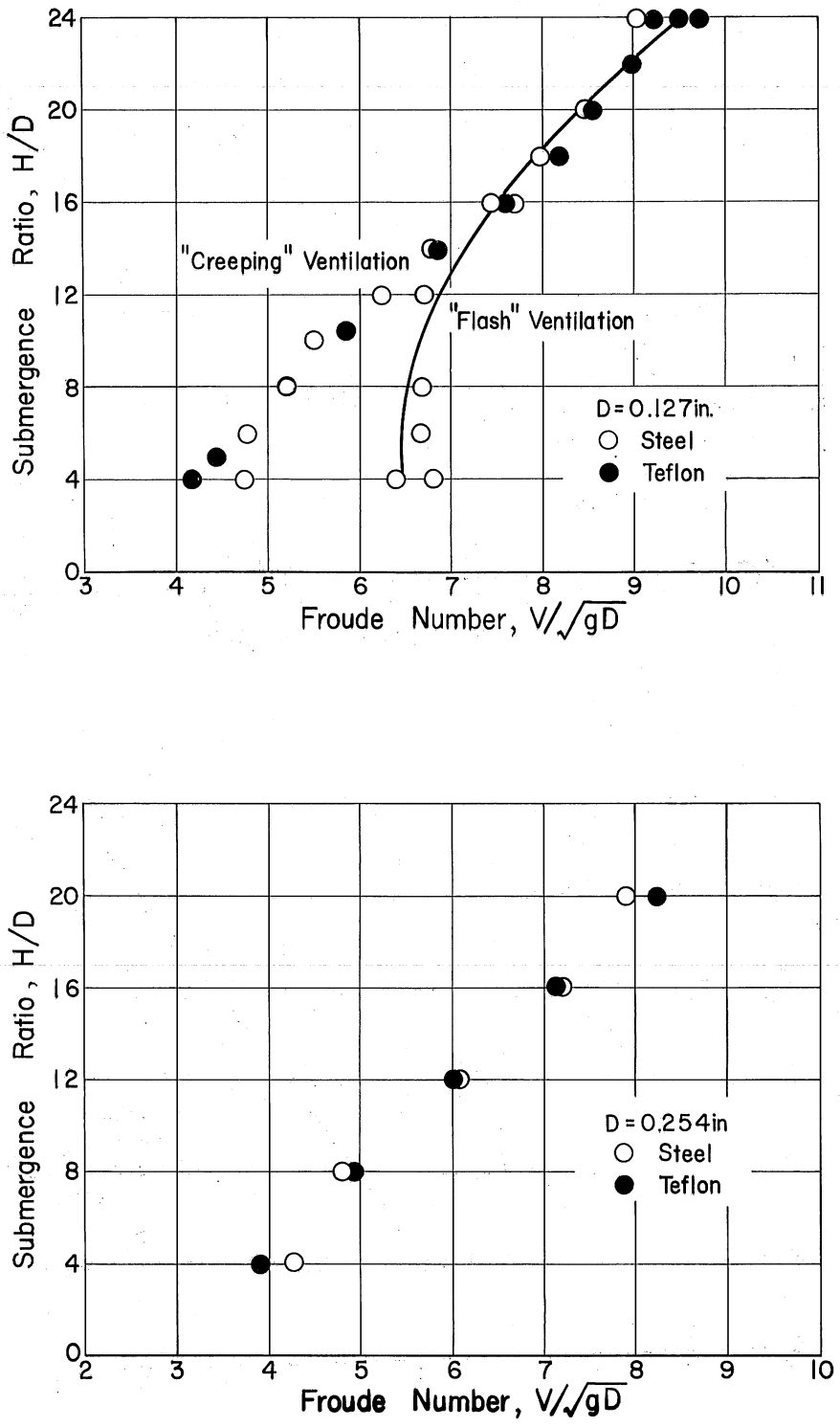

Fig. 17 – Comparison of Creeping and Flash Ventilation Froude Numbers (D = 0.127 and 0.254 in.)

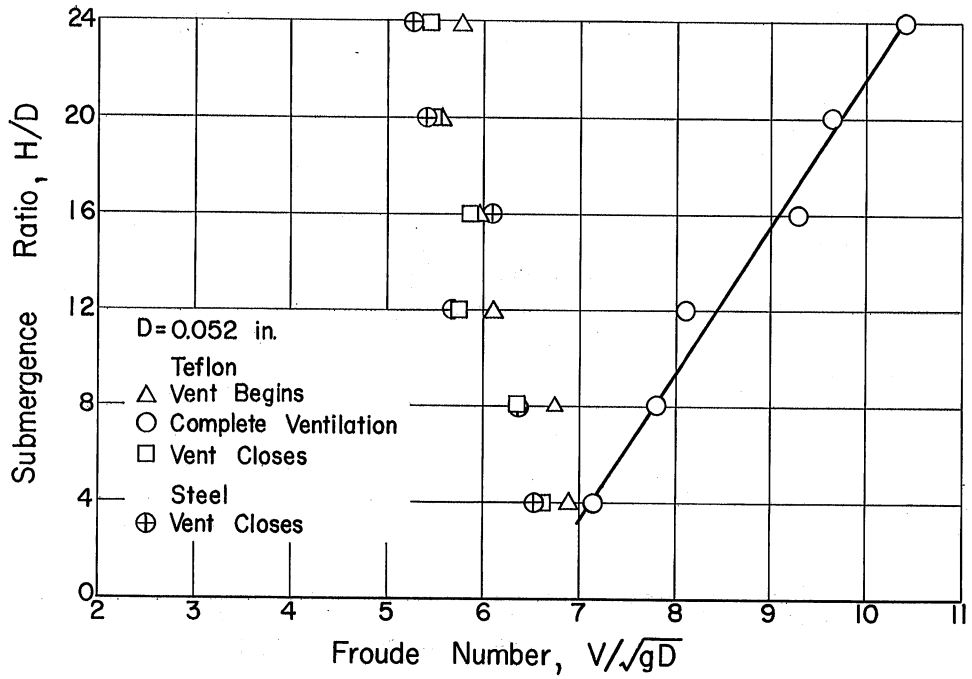

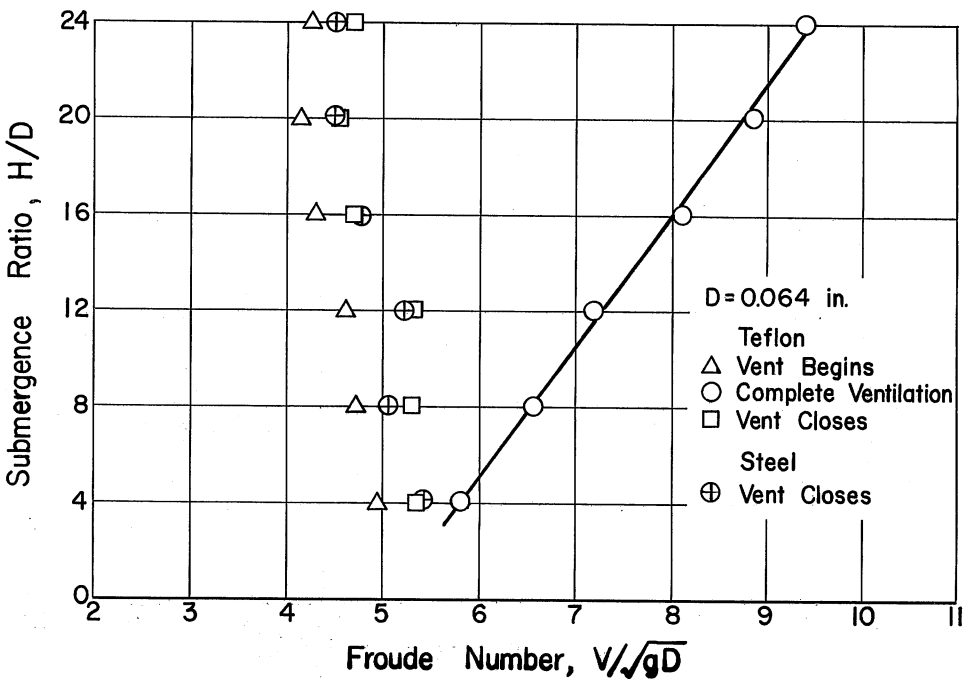

Fig. 18 - Hysteresis Effect on Ventilation of Teflon and Steel Rods (D = 0.052 and 0.064 in.)

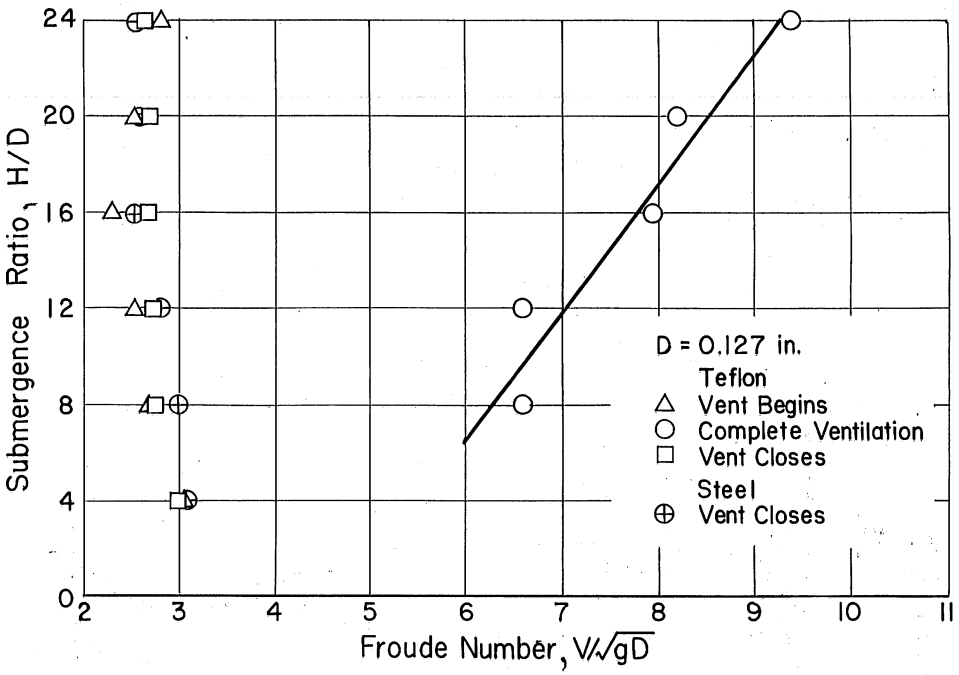

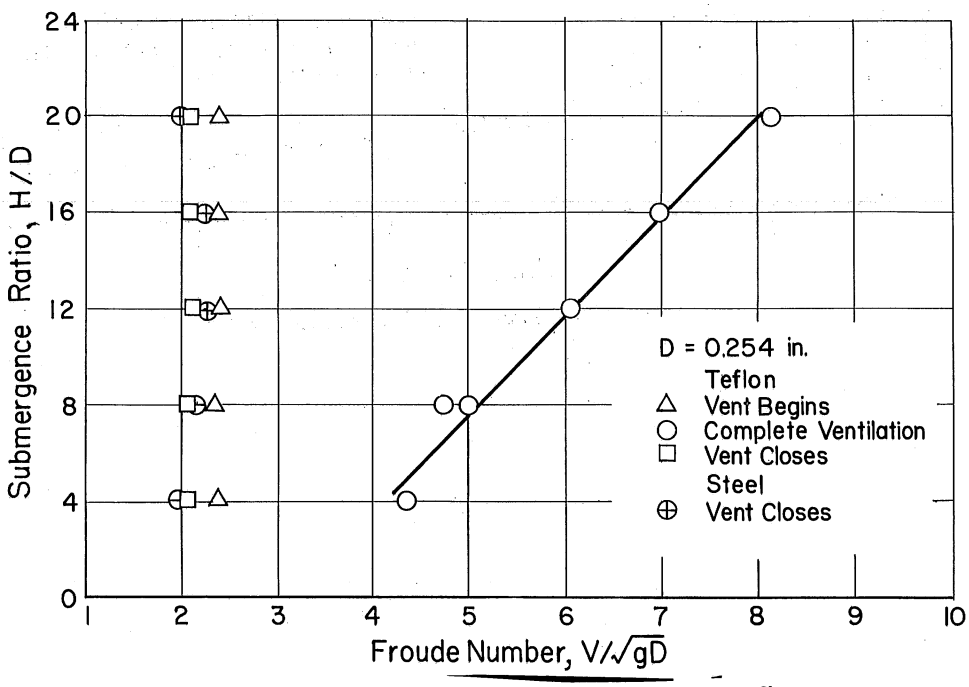

Fig. 19 – Hysteresis Effect on Ventilation of Teflon and Steel Rods (D = 0.127 and 0.254 in.)

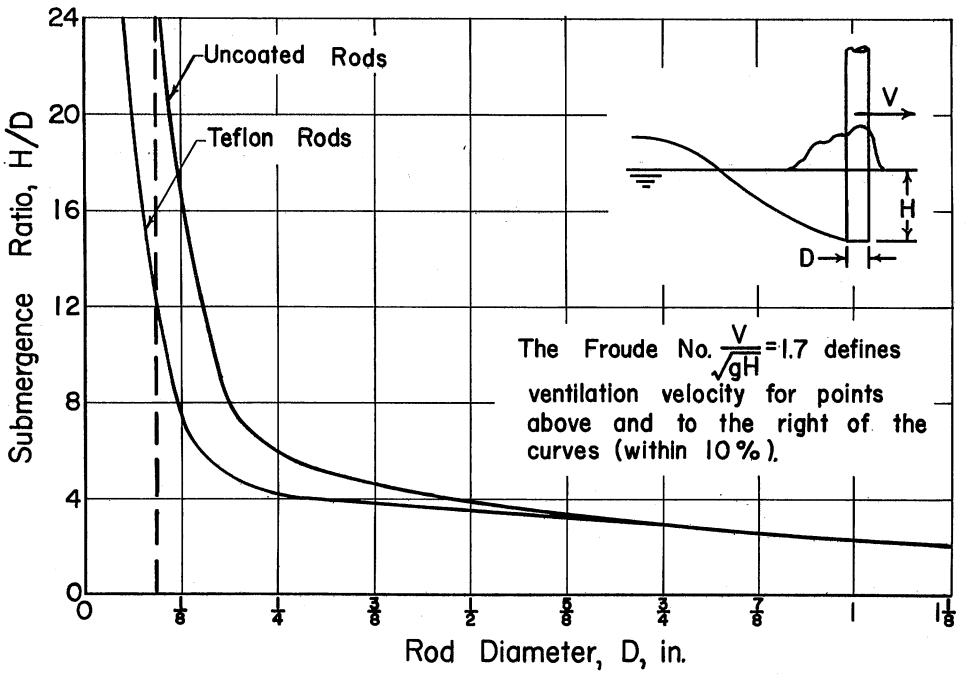

Fig. 20 – Summary of Rod Ventilation Data

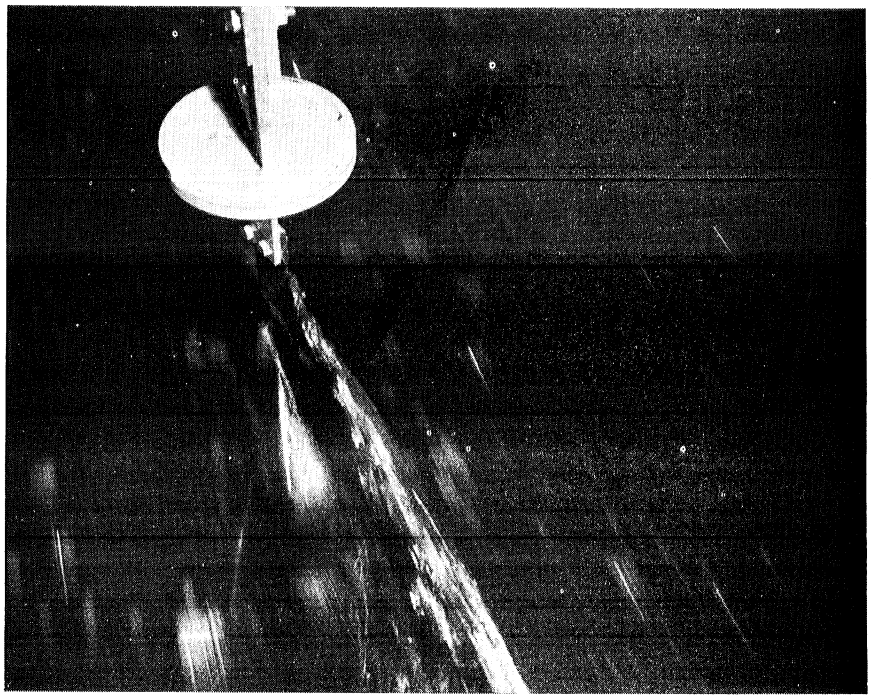

(a) H/C = 4, ψ = 22°, V = 9 fps

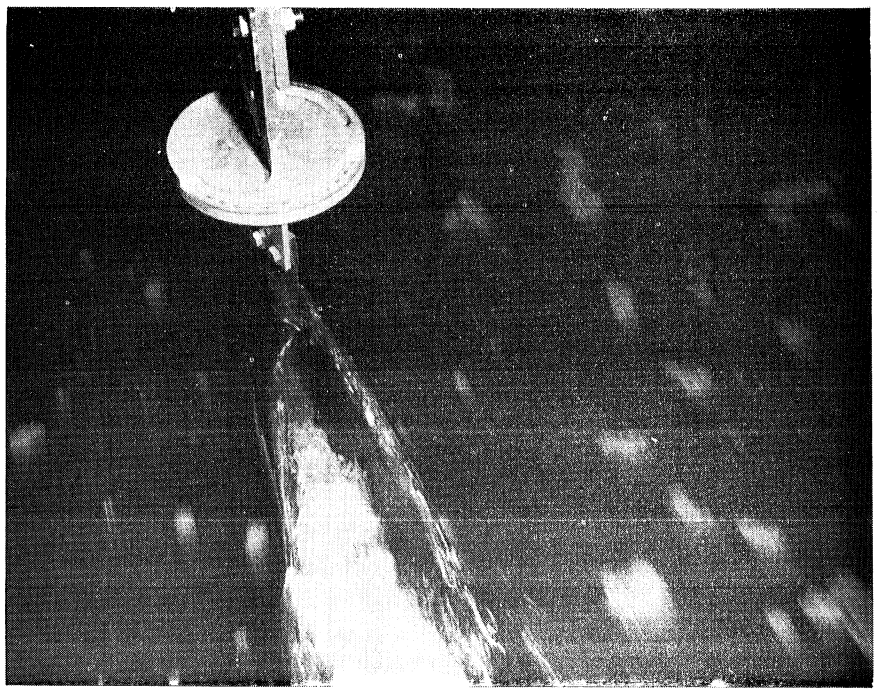

(b) H/C = 4, ψ = 24°, V = 6.5 fps

Fig. 21 - Photographs of Yawed Strut Ventilation

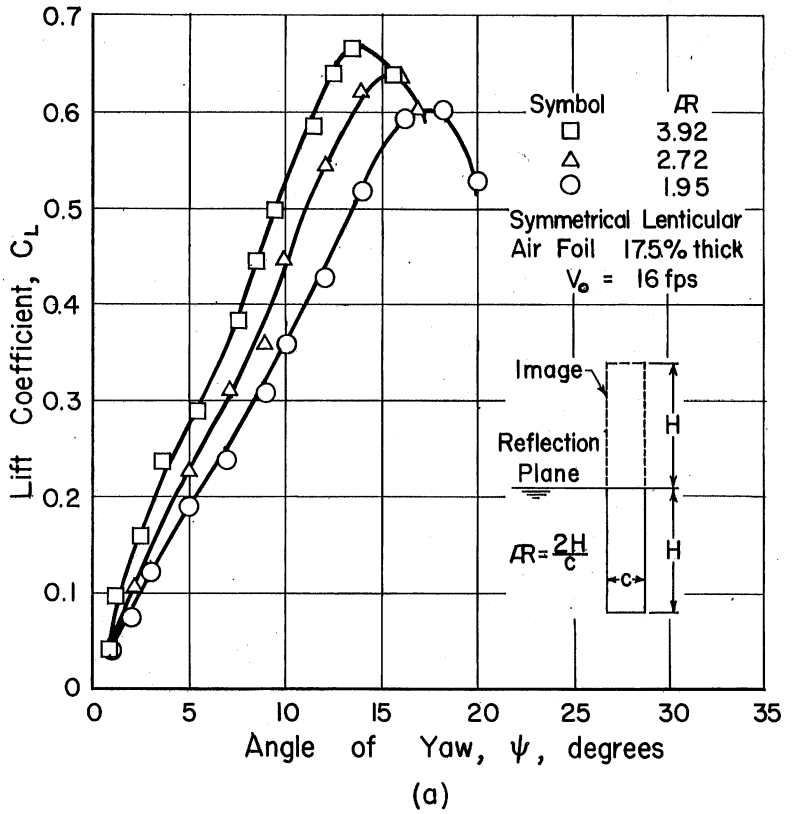

(a)

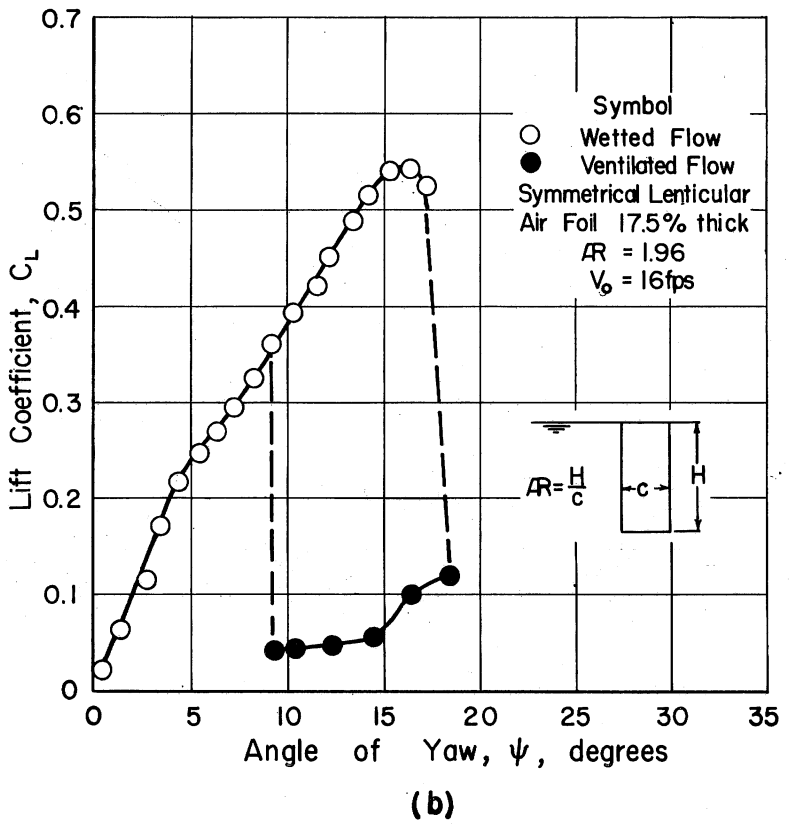

(b)

Fig. 22 – Effect of the Presence of a Free-Surface on the Lift Curve

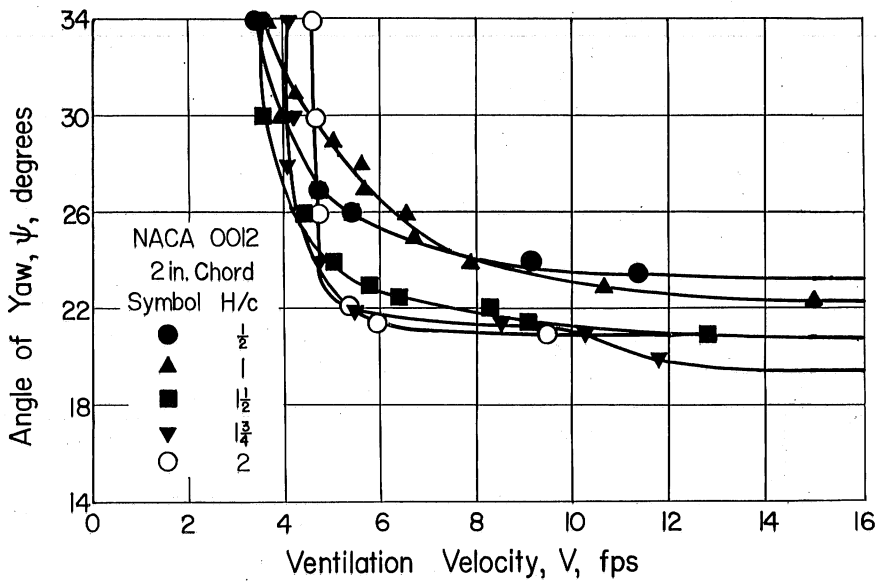

Fig. 23 - Variation of Ventilation Velocity with Yaw Angle and Submergence (NACA 0012)

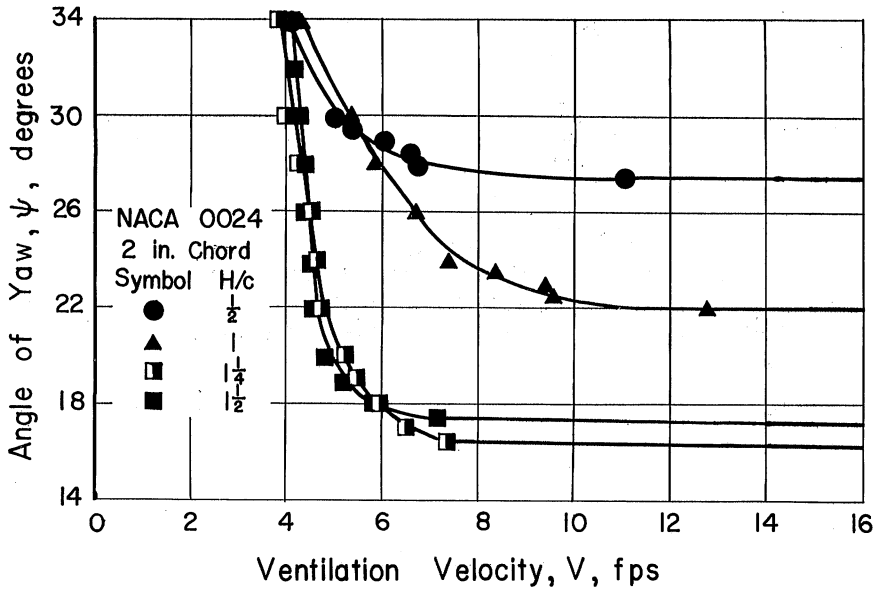

(a)

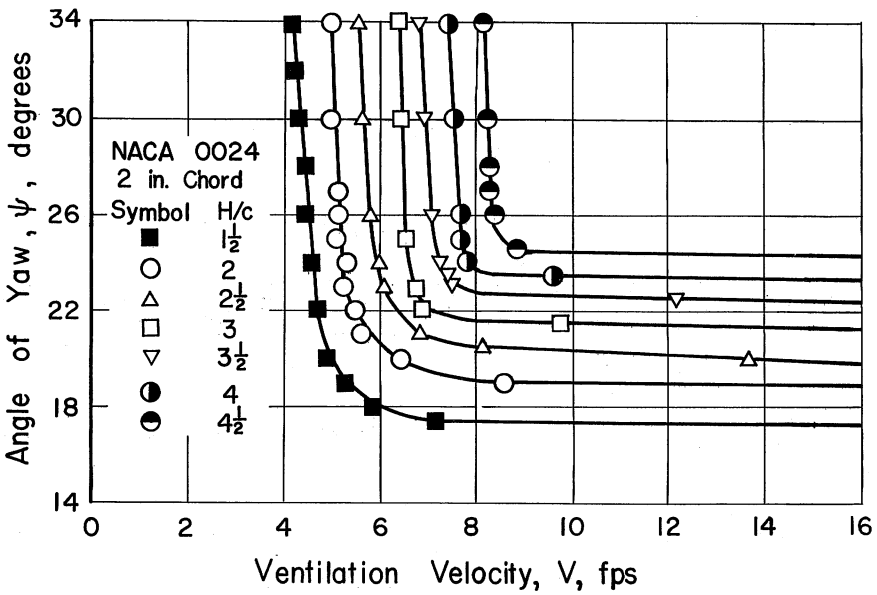

(b)

Fig. 24 - Variation of Ventilation Velocity with Yaw Angle and Submergence (NACA 0024)

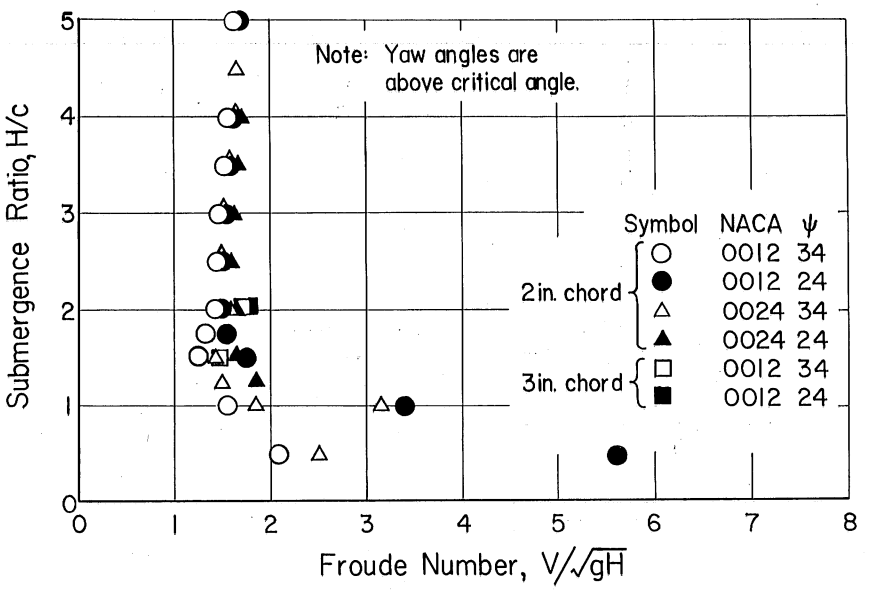

(a)

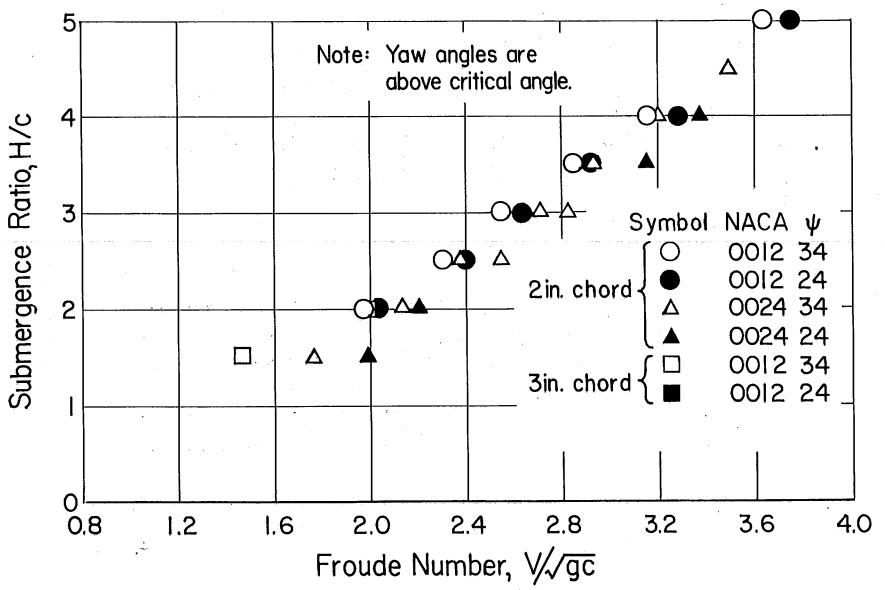

(b)

Fig. 25 - Correlation of High Angle Strut Ventilation Data

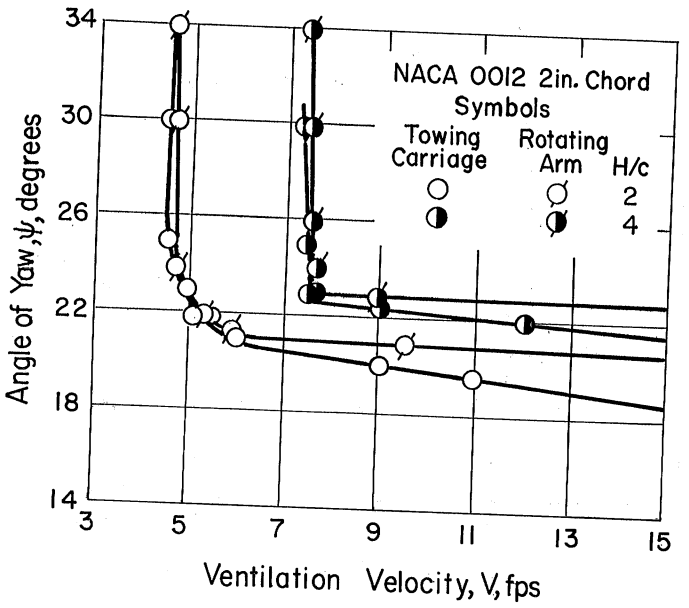

(a)

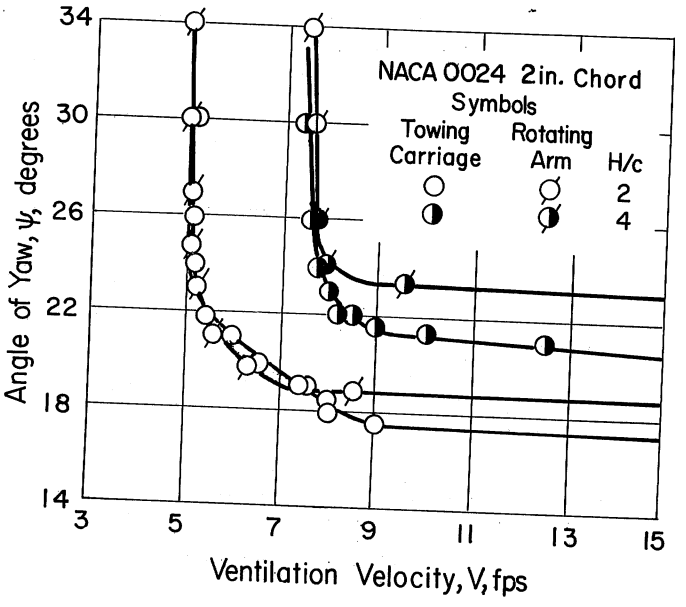

(b)

Fig. 26 – Comparison of Data Taken in Rotating-Arm and Towing Tank Facilities

A P P E N D I X A

PRESSURE DISTRIBUTIONS OF A SURFACE-PIERCING DIHEDRAL HYDROFOIL

APPENDIX A

PRESSURE DISTRIBUTIONS OF A SURFACE-PIERCING DIHEDRAL HYDROFOIL

A. General Considerations

As data were not currently available concerning the pressure distribution on a dihedral hydrofoil, particularly for a dihedral hydrofoil operating in the proximity of a free surface, it appeared that such information might be desirable to assist in the basic understanding of the ventilation phenomena. The previous experimental visual tests indicated that ventilation was primarily a function of dihedral angle, foil shapes, velocity, and angle of attack. There appeared to be a rather small region of instability in which ventilation occurs, and this region could be related experimentally to angle of attack. The pressure distribution studies were conducted to investigate the change of pressure at a particular section and over the foil as a whole, as the zone of instability was approached, for the purpose of finding a reasonable explanation of the triggering mechanism that created the inception of ventilation. The studies were conducted in two facilities, in which subcritical and supercritical flow conditions were obtained as described in the following sections.

B. Experimental Procedure

1. Apparatus

The preliminary tests were conducted in the free-surface water tunnel (Fig. A-1). This facility is a contracted section of a long supply flume. The supply flume is 8 ft wide and 6-1/2 ft deep, the downstream end of the flume contracting to a section 3 ft wide and 6-1/2 ft deep. A high quality of flow with a smooth surface was required for the tests. To meet these requirements, the maximum velocity was limited to 3.5 fps at a depth of about 5.5 ft, resulting in subcritical flow.

Tests at supercritical velocities were conducted in the main test channel, a flume with a clear length of 250 ft, and a 9- by 6-ft cross section. Controllable discharges are obtainable up to 300 cfs with water drawn directly from the Mississippi River. Tests were made in this flume in supercritical flow at velocities of 10.5 fps at a depth of 1.8 ft. A photograph of this facility is also shown in Fig. A-1.

The hydrofoil used for the tests had a rectangular planform with a NACA 0012 section, a span of 16 in. and a chord of 4 inches. It was machined from brass and polished. One limb was slotted longitudinally at various positions along the chord to receive 1/8-in. OD brass tubes extending from the center to the tip of the foil. The tubes were soldered in place and the excess solder removed to form a smooth profile. Number 60 drill holes were located with a 2-in. spacing along the tubes to serve as pressure taps (Fig. A-2). The brass tubes were connected to an air-water manometer used to measure the pressure differentials. The pressure taps were made in one limb only. The entire system placed in the main test channel is shown in Fig. A-3.

To avoid the construction of separate foils for each dihedral angle, the foil was made to receive interchangeable blocks at the center, thereby utilizing the same limbs for each dihedral angle. The interchangeable "V" blocks were made to permit dihedral angles of 15, 30, 45, and 60 degrees. The joints between the blocks and the foil limbs were sealed carefully to prevent leakage. In all cases, the horizontal span of the submerged foil remained unchanged.

2. Test Procedure

The test procedure consisted of measuring the chordwise and spanwise pressure distributions for a given dihedral angle and angle of attack. To permit measurements at each chordwise section, it was necessary to block the other unused pressure taps along the span. Clay was used to seal all holes not being used in the particular test, and proved to be satisfactory. The flow velocity was constant (3.5 fps) for all tests in the free-surface water tunnel, resulting in a Reynolds number (based on chord) of about 0.64×10^5. The flow velocity in the main test channel was 10.5 fps, resulting in a Reynolds number of about 2.6×10^5. The flow velocities and dynamic pressure were measured with a Pitot static tube. The data were plotted for each test in terms of non-dimensional pressure coefficients, defined as $C_p = \frac{P - P_o}{1/2 \rho V_o^2}$ where P = local static pressure, P_o = free stream pressure, and V_o = free stream velocity. The data presented are for 30, 45, and 60 degrees, except that data at subcritical velocities were restricted to dihedral angles of 45 and 60 degrees because of temporarily adverse flow conditions in the test facility.

C. Discussion of Experimental Results

It was not possible to achieve ventilation for most dihedral angles at the velocities available for the tests without resorting to relatively high angles of attack. The NACA 0012 section, which has a high negative pressure peak near the leading edge, was selected since it was found that this section was highly susceptible to flow ventilation. A section with a more uniform pressure distribution has been shown to be less susceptible to ventilation under the same conditions.

As flow at high Froude numbers is of most interest, results of the data for supercritical flow are presented graphically. The data for subcritical flow in general follow the same trends. Tabulated values of C_p for both subcritical and supercritical flow are given at the end of this Appendix. In some cases, the pressure taps were very near the free surface, permitting air to enter the pressure lines. It was not possible to obtain accurate measurements under these conditions.

The pressure coefficients were integrated by planimetering over the pressure diagram to determine the section lift coefficient C_ℓ. Values of C_ℓ are plotted in Fig. A-4 for various positions along the foil limb, to illustrate the distribution of the spanwise load. As the section submergence decreases, the section lift coefficient decreases for a particular angle of attack. The larger angles of attack--and therefore larger measured pressure differences--exhibit less scatter of data.

The chordwise location of the center of pressure has been computed from the pressure coefficients for several angles of attack. As indicated in Fig. A-5 for the 30- and the 45-degree foil, the center of pressure remains essentially near the one-quarter chord point. However, there appears to be a definite trend for the center of pressure to move forward as the submergence of the measuring section is decreased. In some cases, the center of pressure varied with the angle of attack. The variation was not systematic, and further work would be necessary to completely verify any definite conclusions at this point.

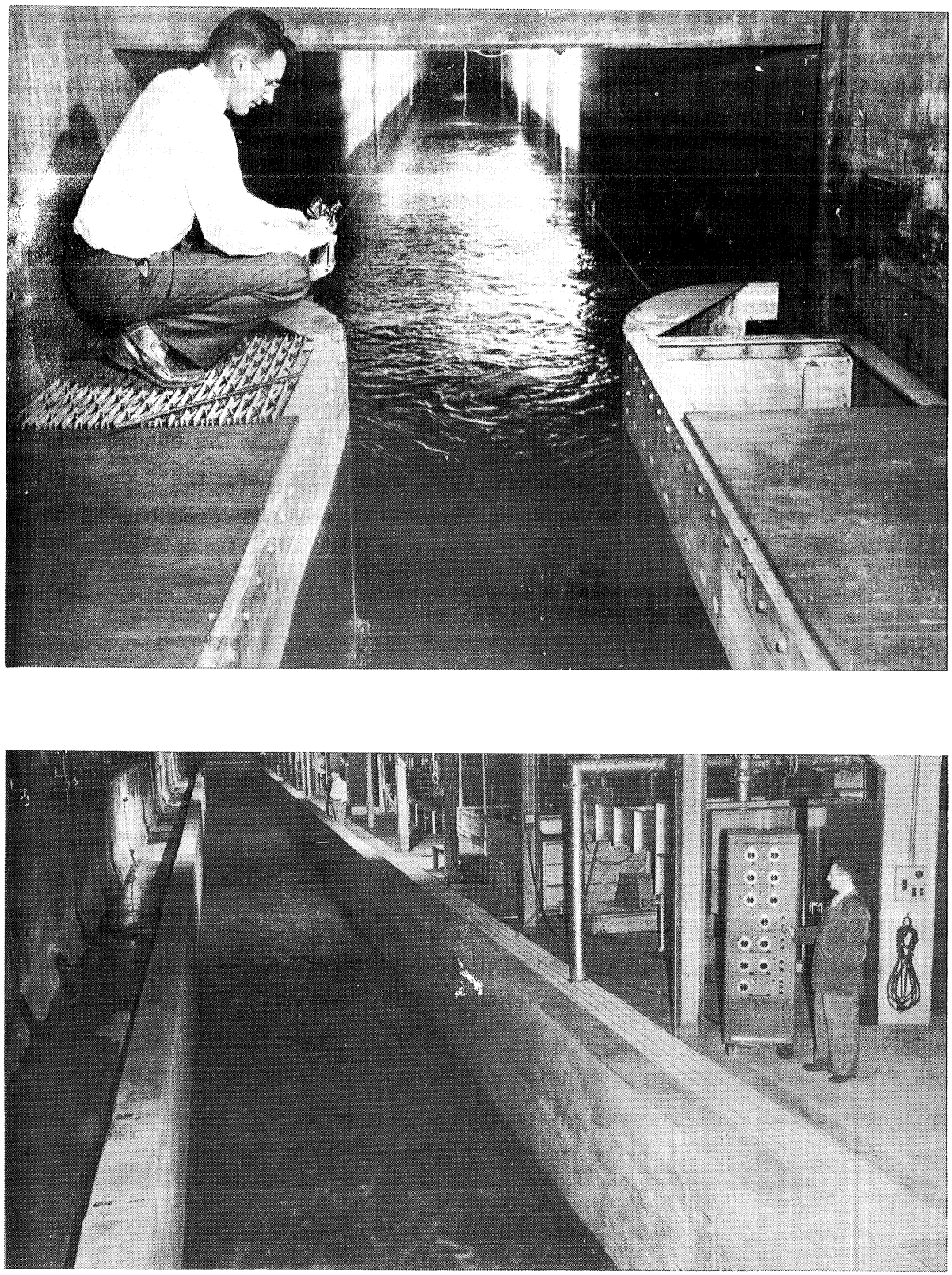

Fig. A-1 – Photographs of Free-Surface Test Facilities

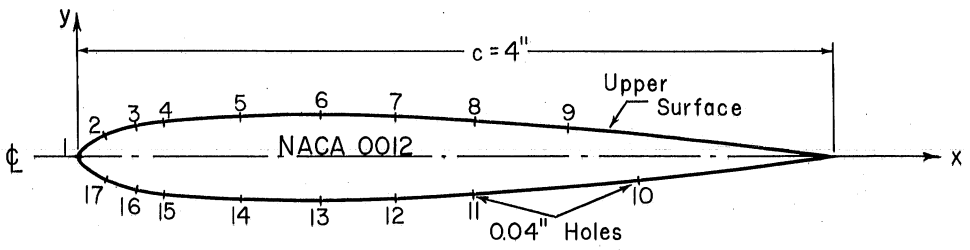

NACA 0012 Coordinates (Symmetrical about ℄)				Piezometer Tap Location		
x (in.)	y (in.)	x (in.)	y (in.)	Tap Number	x/c	y/c
0.000	0.000	1.200	0.2400	1	0.00	0.00
0.050	0.0753	1.600	0.2322	2, 17	3.75	3.09
0.100	0.1046	2.000	0.2118	3, 16	7.50	4.20
0.200	0.1422	2.400	0.1823	4, 15	11.25	4.91
0.300	0.1680	2.800	0.1466	5, 14	21.30	5.79
0.400	0.1874	3.200	0.1052	6, 13	31.30	5.98
0.600	0.2138	3.600	0.0580	7, 12	41.30	5.73
0.800	0.2294	3.800	0.0322	8, 11	51.30	5.22
1.000	0.2376	4.000	0.0050	9	63.80	4.23
				10	72.60	3.42

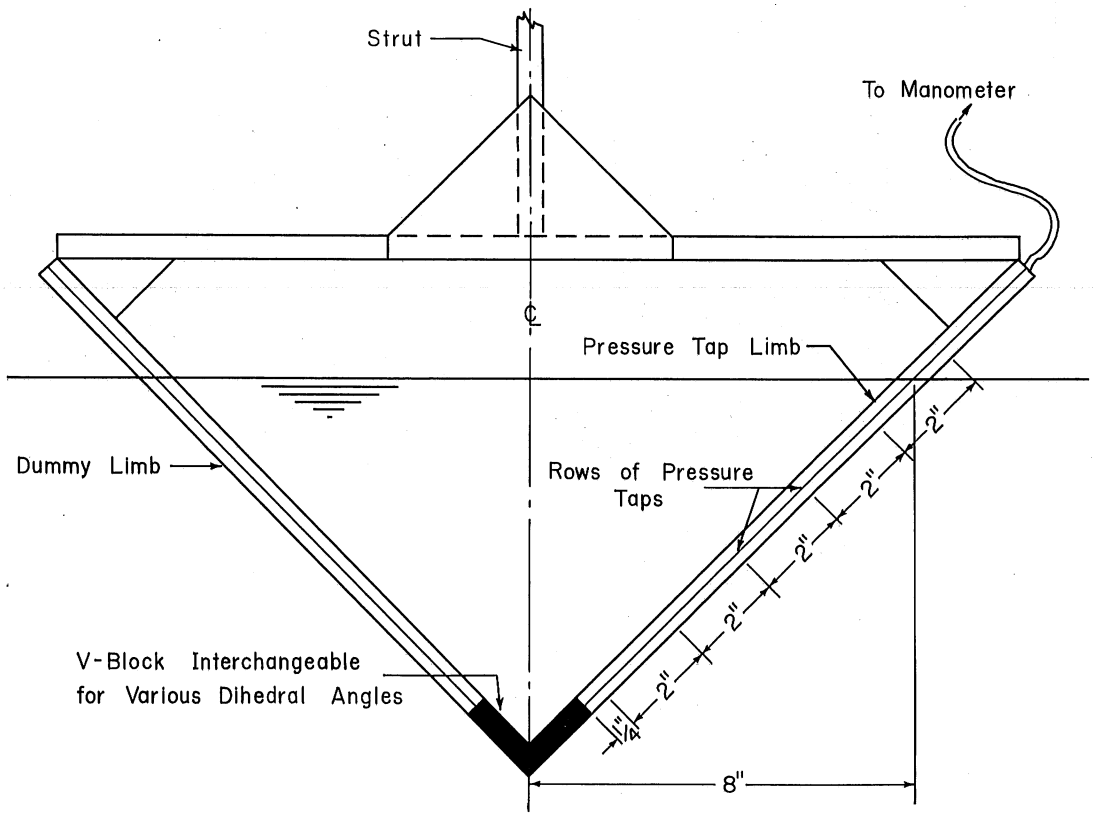

Fig. A-2 – Definition Sketch of Hydrofoil

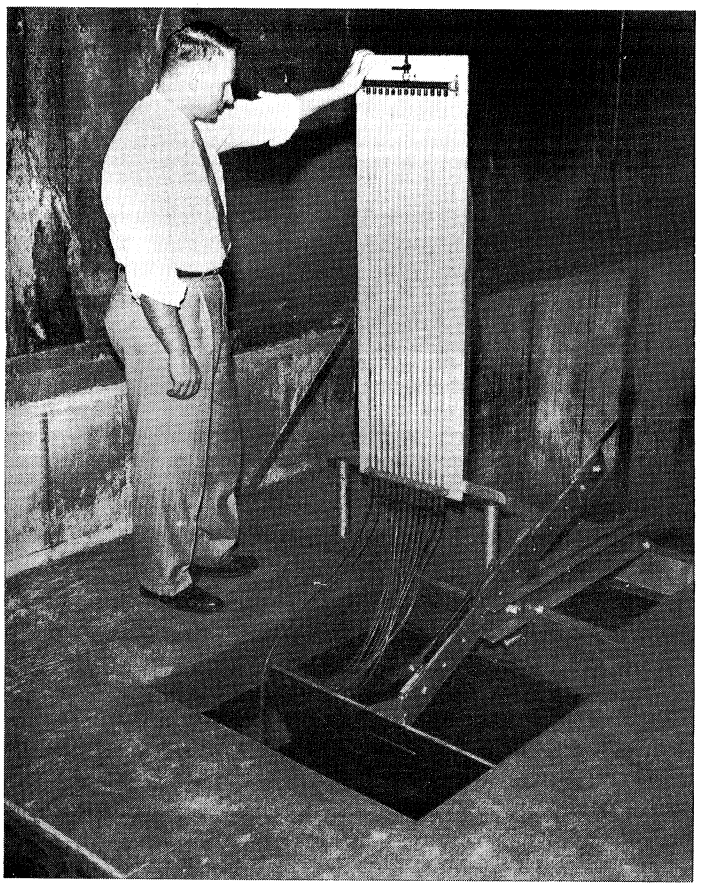

Fig. A-3 - Test Setup in Main Channel

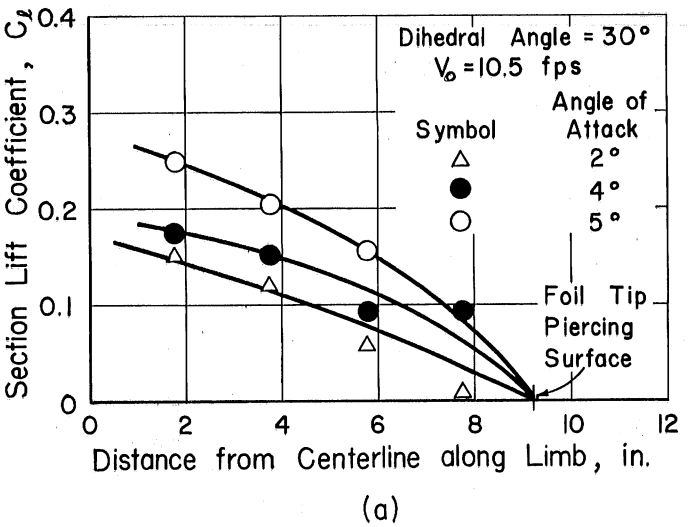

(a)

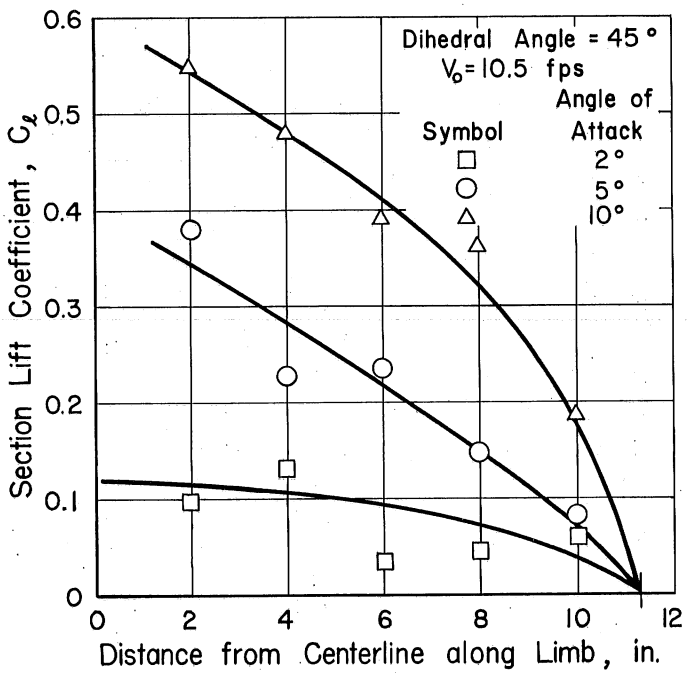

(b)

Fig. A-4 – Spanwise Load Distribution for Dihedral Angles of 30 and 45 Degrees

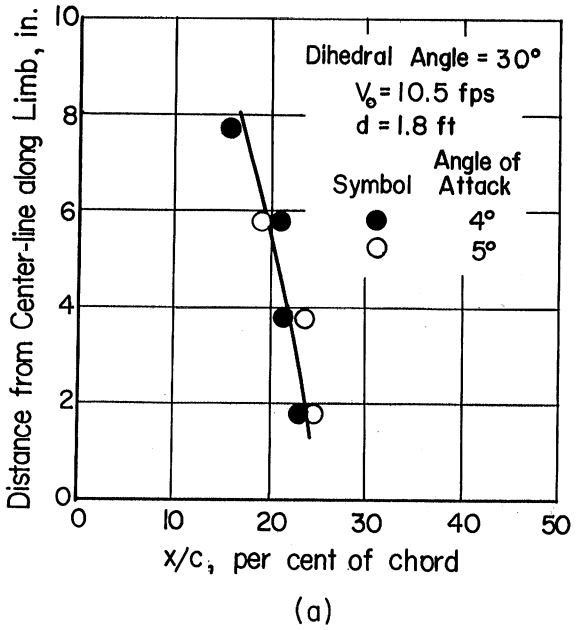

(a)

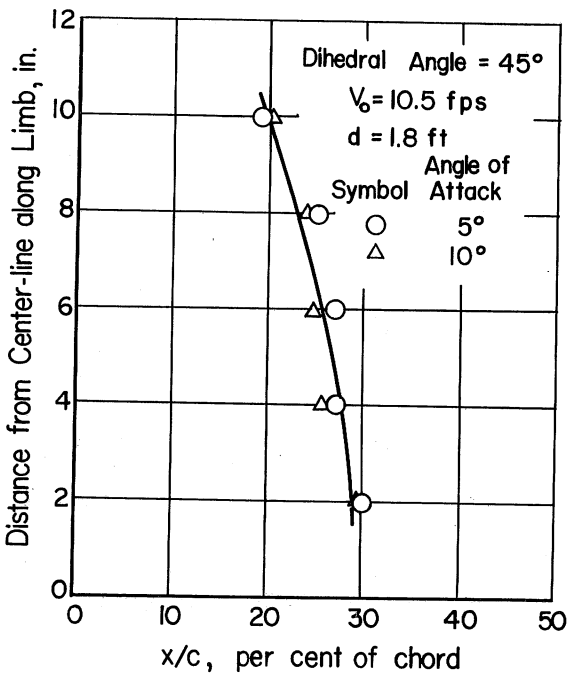

(b)

Fig. A-5 – Chordwise Location of Center of Pressure for Dihedral Angles of 30 and 45 Degrees

A P P E N D I X B

TABULATED PRESSURE DISTRIBUTION DATA

TABULATION OF C_p VALUES

Supercritical Flow

$\gamma = 30^\circ$ $\alpha = 2^\circ$ V = 10.5 fps

Tap No.	CHORD SECTION				
	1	2	3	4	5
1	1.005	1.010	1.02	1.016	
2	-0.372	-0.323	-0.204	-0.253	
3	-0.758	-0.616	-0.564	-0.528	
4	-0.713	-0.688	-0.568	-0.479	
5	-0.561	-0.545	-0.475	-0.316	
6	-0.452	-0.406	-0.361	-0.240	
7	-0.402	-0.377	-0.292	-0.190	
8	-0.331	-0.281	-0.231	-0.140	
9	-0.260	-0.226	-0.166	-0.086	
10	-0.126	-0.117	-0.138	-0.095	
11	-0.234	-0.234	-0.231	-0.240	
12	-0.272	-0.252	-0.288	-0.240	
13	-0.310	-0.289	-0.328	-0.276	
14	-0.306	-0.331	-0.324	-0.303	
15	-0.340	-0.335	-0.346	-0.298	
16	-0.281	-0.214	-0.315	-0.221	
17	-0.042	-0.038	-0.058	-0.050	
C_c	0.022	0.025	0.031	0.026	
C_N	0.151	0.121	0.057	0.009	
C_ℓ	0.150	0.120	0.050	0.008	
C_d	0.0276	0.029	0.033	0.026	

TABULATION OF C_p VALUES

Supercritical Flow

$\gamma = 30^\circ$ $\alpha = 4^\circ$ V = 10.5 fps

Tap No.	CHORD SECTION				
	1	2	3	4	5
1	0.918	0.975	0.964	1.003	
2	-0.365	-0.301	-0.120	-0.349	
3	-0.686	-0.664	-0.587	-0.548	
4	-0.671	-0.700	-0.615	-0.486	
5	-0.506	-0.533	-0.435	-0.316	
6	-0.400	-0.358	-0.348	-0.191	
7	-0.353	-0.338	-0.272	-0.154	
8	-0.298	-0.244	-0.224	-0.138	
9	-0.220	-0.199	-0.156	-0.093	
10	-0.942	-0.094	-0.092	-0.093	
11	-0.1807	-0.211	-0.208	-0.199	
12	-0.220	-0.219	-0.232	-0.211	
13	-0.267	-0.244	-0.260	-0.260	
14	-0.247	-0.260	-0.288	-0.272	
15	-0.275	-0.276	-0.276	-0.255	
16	-0.228	-0.195	-0.224	-0.147	
17	0.416	0.203	0.072	0.120	
C_c	0.028	0.025	0.028	0.024	
C_N	0.174	0.153	0.089	0.093	
C_ℓ	0.172	0.151	0.087	0.091	
C_d	0.040	0.036	0.034	0.030	

TABULATION OF C_p VALUES

Supercritical Flow

	$\gamma = 30^\circ$	$\alpha = 5^\circ$	V = 10.5 fps		
Tap No.	CHORD SECTION				
	1	2	3	4	5
1	1.01	1.05	1.07		
2	-0.69	-0.474	-0.477		
3	-1.02	-0.831	-0.768		
4	-0.896	-0.81	-0.806		
5	-0.606	-0.666	-0.506		
6	-0.468	-0.44	-0.42		
7	-0.423	-0.426	-0.334		
8	-0.363	-0.304	-0.262		
9	-0.267	-0.261	-0.191		
10	-0.101	-0.105	-0.11		
11	-0.225	-0.239	-0.22		
12	-0.239	-0.218	-0.239		
13	-0.257	-0.257	-0.253		
14	-0.234	-0.257	-0.305		
15	-0.216	-0.244	-0.234		
16	-0.138	-0.13	-0.129		
17	0.183	0.122	0.181		
C_c	0.008	0.017	0.017		
C_N	0.247	0.204	0.156		
C_ℓ	0.246	0.202	0.154		
C_d	0.030	0.035	0.030		

TABULATION OF C_p VALUES

Supercritical Flow

	$\gamma = 45^\circ$	$\alpha = 2^\circ$		V = 10.5 fps	
Tap No.	CHORD SECTION				
	1	2	3	4	5
1	1.06	1.045	1.08	1.11	1.15
2	-0.131	-0.17	-0.025	-0.136	-0.448
3	-0.62	-0.618	-0.465	-0.515	-0.683
4	-0.642	-0.695	-0.57	-0.515	-0.542
5	-0.545	-0.603	-0.45	-0.455	-0.41
6	-0.48	-0.417	-0.425	-0.414	-0.36
7	-0.465	-0.437	-0.351	-0.374	-0.30
8	-0.409	-0.324	-0.307	-0.318	-0.224
9	-0.328	-0.288	-0.228	-0.232	-0.191
10	-0.136	-0.124	-0.143	-0.136	-0.164
11	-0.298	-0.304	-0.312	-0.256	-0.322
12	-0.343	-0.293	-0.376	-0.313	-0.312
13	-0.384	-0.345	-0.376	-0.389	-0.317
14	-0.404	-0.386	-0.465	-0.44	-0.355
15	-0.47	-0.35	-0.475	-0.45	-0.328
16	-0.43	-0.155	-0.465	-0.389	-0.247
17	-0.212	0.005	-0.198	-0.131	0.072
C_c	0.017	0.023	0.027	0.020	0.0221
C_N	0.095	0.129	0.031	0.043	0.057
C_ℓ	0.095	0.129	0.038	0.043	0.057
C_d	0.020	0.027	0.029	0.021	0.024

TABULATION OF C_p VALUES

Supercritical Flow

$\gamma = 45^{\circ}$ $\alpha = 5^{\circ}$ V = 10.5 fps

Tap No.	CHORD SECTION				
	1	2	3	4	5
1	1.065	1.090	0.930	1.135	1.160
2	-0.485	-0.353	-0.488	-0.315	-0.277
3	-0.841	-0.726	-0.814	-0.630	-0.640
4	-0.841	-0.765	-0.804	-0.582	-0.540
5	-0.639	-0.663	-0.556	-0.448	-0.342
6	-0.545	-0.411	-0.468	-0.386	-0.252
7	-0.445	-0.436	-0.370	-0.324	-0.188
8	-0.406	-0.295	-0.309	-0.210	-0.144
9	-0.312	-0.237	-0.180	-0.186	-0.094
10	-0.069	-0.068	-0.004	-0.029	-0.035
11	-0.016	-0.208	-0.175	-0.148	-0.109
12	-0.022	-0.203	-0.201	-0.186	-0.149
13	-0.023	-0.218	-0.206	-0.243	-0.203
14	-0.023	-0.261	-0.232	-0.258	-0.252
15	-0.019	-0.257	-0.105	-0.253	-0.208
16	-0.011	-0.135	-0.011	-0.200	-0.193
17	0.163	-0.179	0.378	0.105	0.074
C_c	0.024	0.027	0.034	0.026	0.021
C_N	0.383	0.227	0.238	0.148	0.083
C_ℓ	0.380	0.224	0.234	0.145	0.080
C_d	0.058	0.046	0.055	0.039	0.028

TABULATION OF C_p VALUES

Supercritical Flow

	$\gamma = 45^\circ$	$\alpha = 10^\circ$		V = 10.5 fps	
Tap No.	CHORD SECTION				
	1	2	3	4	5
1	0.842	0.763	0.525	0.818	0.948
2	-1.49	-1.17	-1.11	-1.08	-0.625
3	-1.65	-1.34	-1.23	-1.07	-0.786
4	-1.40	-1.22	-1.13	-0.925	-0.696
5	-0.915	-0.964	-0.733	-0.69	-0.448
6	-0.742	-0.63	-0.624	-0.60	-0.372
7	-0.658	-0.577	-0.49	-0.47	-0.286
8	-0.530	-0.42	-0.411	-0.382	-0.215
9	-0.376	-0.334	-0.272	-0.248	-0.176
10	-0.064	-0.043	-0.064	-0.069	-0.086
11	-0.104	-0.124	-0.148	-0.13	-0.153
12	-0.144	-0.119	-0.154	-0.143	-0.219
13	-0.109	-0.105	-0.129	-0.161	-0.186
14	-0.069	-0.067	-0.139	-0.11	-0.20
15	-0.015	0	0.05	-0.106	-0.138
16	0.163	0.153	0.193	0.083	0.009
17	0.575	0.515	0.56	0.39	0.348
C_c	-0.012	-0.004	0.003	0.002	0.128
C_N	0.552	0.485	0.396	0.368	0.189
C_ℓ	0.546	0.478	0.390	0.362	0.184
C_d	0.084	0.080	0.072	0.066	0.045

TABULATION OF C_p VALUES

Subcritical Flow

	$\gamma = 30^\circ$	$\alpha = 2^\circ$	V = 3.5 fps		
Tap No.	CHORD SECTION				
	1	2	3	4	5
1	0.875	1.05	0.524	0.546	
2	-0.218	-0.830	-1.13	-0.981	
3	-0.567	-1.04	-1.02	-0.874	
4	-0.765	-0.960	-0.874	-0.654	
5	-0.497	-0.722	-0.612	-0.502	
6	-0.481	-0.525	-0.393	-0.284	
7	-0.437	-0.392	-0.262	-0.125	
8	-0.350	-0.284	-0.197	-0.153	
9	-0.262	-0.240	-0.175	-0.109	
10	-0.044	-0.066	-0.044	-0.066	
11	-0.175	-0.131	-0.111	-0.109	
12	-0.227	-0.175	-0.111	-0.109	
13	-0.306	-0.175	-0.088	-0.109	
14	-0.372	-0.131	-0.044	-0.039	
15	-0.372	-0.044	-0.111	0.144	
16	-0.437	0.175	0.306	0.328	
17	-0.393	0.459	0.634	0.678	
C_c	-0.008	-0.028	-0.002	-0.008	
C_N	0.149	0.322	0.327	0.259	
C_ℓ	0.149	0.322	0.327	0.259	
C_d	-0.003	-0.017	0.009	0.001	

TABULATION OF C_p VALUES

Subcritical Flow

	$\gamma = 30^\circ$	$\alpha = 5^\circ$	V = 3.5 fps		
Tap No.	CHORD SECTION				
	1	2	3	4	5
1	1.09	0.700	0.022	0.000	
2	-0.872	-0.720	-1.40	-0.915	
3	-1.31	-1.01	-1.27	-0.675	
4	-0.655	-0.930	-1.07	-0.567	
5	-0.458	-0.632	-0.634	-0.546	
6	-0.335	-0.437	-0.425	-0.305	
7	-0.249	-0.310	-0.328	-0.262	
8	-0.175	-0.240	-0.262	-0.218	
9	-0.109	-0.153	-0.219	-0.200	
10	0.022	-0.022	0.110	-0.176	
11	-0.044	-0.083	-0.153	-0.176	
12	-0.088	-0.096	-0.153	-0.153	
13	-0.088	-0.096	-0.153	-0.109	
14	-0.066	-0.065	-0.110	-0.044	
15	-0.000	-0.000	0.022	0.218	
16	0.066	0.175	0.036	0.437	
17	0.480	0.372	0.742	0.786	
C_c	-0.00813	-0.00581	0.024	-0.0199	
C_N	0.264	0.315	0.364	0.261	
C_ℓ	0.264	0.314	-0.360	0.217	
C_d	0.015	0.022	0.056	-0.002	

TABULATION OF C_p VALUES

Subcritical Flow

$\gamma = 45^\circ$ $\alpha = 5^\circ$ V = 3.5 fps

Tap No.	CHORD SECTION				
	1	2	3	4	5
1	0.935	0.830	0.570	0.350	0.328
2	-0.96	-0.960	-1.24	-1.30	-0.844
3	-1.15	-1.14	-1.24	-1.09	-0.744
4	-1.025	-1.06	-1.18	-0.765	-0.525
5	-0.72	-0.830	-0.96	-0.790	-0.415
6	-0.623	-0.698	-0.807	-0.555	-0.175
7	-0.531	-0.590	-0.642	-0.41	-0.130
8	-0.465	-0.480	-0.502	-0.314	-0.130
9	-0.392	-0.393	-0.392	-0.262	-0.096
10	-0.131	-0.109	-0.174	-0.087	-0.088
11	-0.174	-0.197	-0.218	-0.109	-0.088
12	-0.183	-0.197	-0.231	-0.109	-0.079
13	-0.174	-0.197	-0.231	-0.096	-0.057
14	-0.166	-0.175	-0.218	-0.057	-0.022
15	-0.065	-0.022	-0.022	0.109	0.175
16	0.087	0.088	0.210	0.306	0.35
17	0.415	0.393	0.560	0.655	0.735
C_c	0.023	0.018	-0.004	-0.013	0.004
C_N	0.359	0.420	0.467	0.418	0.209
C_ℓ	0.346	0.416	0.465	0.417	0.208
C_d	0.055	0.055	0.037	0.023	0.014

TABULATION OF C_p VALUES

Subcritical Flow

$\gamma = 45^\circ$ $\alpha = 10^\circ$ V = 3.5 fps

Tap No.	CHORD SECTION				
	1	2	3	4	5
1	1.090	0.788	0.218	-0.262	-0.066
2	-1.18	-1.33	-1.4	-1.60	-0.862
3	-1.05	-1.14	-1.49	-1.31	-0.875
4	-1.05	-1.38	-1.31	-1.19	-0.722
5	-0.895	-0.985	-1.03	-0.765	-0.424
6	-0.75	-0.830	-0.788	-0.468	-0.262
7	-0.655	-0.656	-0.612	-0.394	-0.236
8	-0.59	-0.525	-0.481	-0.328	-0.249
9	-0.525	-0.394	-0.372	-0.262	-0.219
10	-0.197	-0.0875	-0.109	-0.109	-0.109
11	-0.218	-0.131	-0.131	-0.088	-0.070
12	-0.240	-0.131	-0.131	-0.075	-0.053
13	-0.218	-0.131	-0.118	-0.057	-0.044
14	-0.175	-0.088	-0.109	0	0.044
15	-0.066	0.088	0.109	0.240	0.262
16	0.109	0.218	0.306	0.415	0.350
17	0.460	0.655	0.612	0.744	0.788
C_c	0.025	0.019	-0.016	-0.030	-0.001
C_N	0.483	0.542	0.553	0.504	0.338
C_ℓ	0.471	0.532	0.548	0.491	0.333
C_d	0.109	0.113	0.081	0.058	0.057

TABULATION OF C_p VALUES

Subcritical Flow

$\gamma = 45^\circ$	$\alpha = 15^\circ$	V = 3.5 fps		
Tap No.	CHORD SECTION			
	1	2	3	4	5
1	0.079	-0.044	-0.875	-1.095	-0.535
2	-1.64	-1.87	-2.01	-1.925	-1.530
3	-1.44	-1.65	-1.44	-1.560	-1.005
4	-1.27	-1.485	-1.63	-1.375	-0.788
5	-1.01	-1.05	-1.16	-0.788	-0.393
6	-0.63	-0.678	-0.678	-0.533	-0.262
7	-0.512	-0.547	-0.546	-0.437	-0.197
8	-0.515	-0.437	-0.402	-0.349	-0.179
9	-0.498	-0.315	-0.284	-0.262	-0.179
10	-0.105	-0.026	0	-0.30	-0.87
11	-0.061	-0.026	0	-0.009	0.061
12	-0.48	-0.013	0.044	0.022	0.088
13	-0.008	0.044	0.088	0.066	0.119
14	0.088	0.118	0.175	0.157	0.254
15	0.262	0.328	0.460	0.524	0.473
16	0.568	0.490	0.647	0.656	0.644
17	0.787	0.832	0.915	0.963	1.00
C_c	-0.011	-0.042	-0.056	-0.060	-0.031
C_N	0.690	0.683	0.680	0.660	0.490
C_ℓ	0.669	0.670	0.671	0.654	0.481
C_d	0.168	0.137	0.123	0.113	0.097

TABULATION OF C_p VALUES

Subcritical Flow

$\gamma = 45^\circ$	$\alpha = 21^\circ$	V = 3.5 fps		
Tap No.	CHORD SECTION			
	1	2	3	4	5
1	-1.01	-1.49	-1.57	-1.22	-1.24
2	-2.27	-2.29	-1.72	-1.74	-1.59
3	-1.79	-1.85	-1.35	-1.37	-1.35
4	-1.61	-1.68	-1.63	-1.24	-0.83
5	-1.135	-1.2	-1.03	-0.990	-0.61
6	-0.720	-0.850	-0.83	-0.830	-0.427
7	-0.655	-0.696	-0.687	-0.655	-0.327
8	-0.698	-0.565	-0.524	-0.523	-0.27
9	-0.764	-0.443	-0.371	-0.393	-0.262
10	-0.153	-0.044	-0.044	-0.022	-0.044
11	-0.053	0.022	0.035	0.057	0.065
12	0	0.065	0.098	0.131	0.088
13	0.078	0.13	0.175	0.197	0.174
14	0.153	0.253	0.306	0.349	0.327
15	0.458	0.521	0.568	0.567	0.602
16	1.05	0.718	0.740	0.742	0.784
17	0.940	0.915	0.960	0.913	0.928
C_c	-0.038	-0.070	-0.058	-0.052	-0.056
C_N	0.950	0.908	0.842	0.811	0.577
C_ℓ	0.902	0.873	0.806	0.776	0.559
C_d	0.304	0.259	0.248	0.241	0.154

TABULATION OF C_p VALUES

Subcritical Flow

$\gamma = 60^\circ$ $\alpha = 5^\circ$ V = 3.5 fps

Tap No.	CHORD SECTION					
	1	2	3	4	5	6
1	1.04	1.01	1.01	0.940	0.805	0.700
2	-0.218	-0.339	-0.328	-0.371	-0.545	-0.611
3	-0.572	-0.698	-0.740	-0.852	-0.785	-0.462
4	-0.610	-0.654	-0.721	-0.707	-0.654	-0.524
5	-0.727	-0.600	-0.457	-0.458	-0.460	-0.371
6	-0.597	-0.490	-0.394	-0.393	-0.372	-0.340
7	-0.532	-0.415	-0.306	-0.319	-0.297	-0.222
8	-0.487	-0.349	-0.262	-0.240	-0.240	-0.144
9	-0.445	-0.292	-0.230	-0.175	-0.153	-0.079
10	-0.205	-0.057	-0.022	0	-0.022	-0.018
11	-0.293	-0.162	-0.087	-0.066	-0.074	-0.044
12	-0.336	-0.205	-0.131	-0.079	-0.109	-0.066
13	-0.349	-0.240	-0.162	-0.101	-0.109	-0.066
14	-0.336	-0.240	-0.170	-0.096	-0.074	-0.035
15	-0.336	-0.109	-0.065	0	-0.065	0.066
16	-0.066	-0.100	0.087	0.196	0.166	0.153
17	0.131	0.197	0.197	0.490	0.480	0.590
C_c	0.039	0.021	0.019	0.030	0.021	0.016
C_N	0.211	0.256	0.262	0.276	0.245	0.227
C_ℓ	0.207	0.253	0.259	0.272	0.238	0.225
C_d	0.057	0.043	0.042	0.054	0.042	0.035

TABULATION OF C_p VALUES

Subcritical Flow

$\gamma = 60^\circ$ $\alpha = 10^\circ$ V = 3.5 fps

Tap No.	CHORD SECTION					
	1	2	3	4	5	6
1	0.107	0.842	0.805	0.456	0.328	0.478
2	-0.523	-0.910	-0.652	-1.040	-0.995	-0.76
3	-0.830	-1.07	-1.35	-1.050	-1.02	-0.542
4	-0.810	-0.900	-0.87	-0.958	-0.804	-0.50
5	-0.644	-0.750	-0.682	-0.696	-0.587	-0.392
6	-0.524	-0.620	-0.574	-0.566	-0.414	-0.218
7	-0.467	-0.524	-0.470	-0.437	-0.296	-0.139
8	-0.393	-0.402	-0.370	-0.350	-0.218	-0.131
9	-0.349	-0.292	-0.227	-0.262	-0.161	-0.131
10	-0.153	-0.052	-0.009	-0.031	0	-0.044
11	-0.125	-0.127	-0.096	-0.087	-0.044	-0.022
12	-0.197	-0.143	-0.117	-0.109	-0.044	-0.004
13	-0.175	-0.143	-0.117	-0.109	-0.022	0.022
14	-0.175	-0.143	-0.087	-0.087	0.022	0.083
15	-0.122	0		0	0.196	0.240
16	0	0.156	0.196	0.284	0.366	0.358
17	0.262	0.524	0.544	0.650	0.925	0.610
C_c	0.026	0.0108	0.014	0.013	0	0.006
C_N	0.292	0.376	0.379	0.414	0.384	0.259
C_ℓ	0.284	0.369	0.371	0.406	0.378	0.255
C_d	0.076	0.076	0.080	0.085	0.067	0.051

TABULATION OF C_p VALUES

Subcritical Flow

$\gamma = 60^\circ$ $\alpha = 15^\circ$ V = 3.5 fps

Tap No.	CHORD SECTION					
	1	2	3	4	5	6
1	0.810	0.415	0.044	-0.131	-0.393	0.066
2	-1.03	-1.30	-1.49	-1.42	-1.57	-1.74
3	-1.18	-1.35	-1.35	-1.36	-1.44	
4	-1.05	-1.22	-1.17	-1.20	-1.05	
5	-0.80	-0.852	-0.875	-0.95	-0.895	-0.802
6	-0.67	-0.743	-0.713	-0.612	-0.502	-0.567
7	-0.582	-0.503	-0.503	-0.406	-0.393	-0.480
8	-0.494	-0.371	-0.367	-0.350	-0.319	-0.414
9	-0.560	-0.284	-0.262	-0.284	-0.240	-0.349
10	-0.188	-0.031	-0.013	0	-0.022	-0.152
11	-0.166	-0.057	-0.035	0.022	-0.022	-0.131
12	-0.166	-0.057	-0.035	0	0	-0.109
13	-0.144	-0.057	-0.013	0.013	0.044	-0.057
14	-0.101	0	0.048	0.101	0.131	0
15	0.031	0.175	0.205	0.275	0.328	0.196
16	0.197	0.297	0.372	0.450	0.807	0.414
17	0.525	0.656	0.786	0.787	0.916	0.458
C_c	0.024	-0.013	-0.025	-0.027	-0.034	-0.032
C_N	0.495	0.542	0.595	0.592	0.600	0.532
C_ℓ	0.471	0.526	0.581	0.578	0.589	0.522
C_d	0.152	0.128	0.130	0.128	0.122	0.107

TABULATION OF C_p VALUES

Subcritical Flow

$\gamma = 60$ $\alpha = 20^{\circ}$ V = 3.5 fps

Tap No.	CHORD SECTION					
	1	2	3	4	5	6
1	0.293	-0.131	-0.808	-0.437	-0.70	-1.38
2	-1.600	-1.75	-1.86	-2.01	-1.75	-1.40
3	-1.38	-1.53	-1.79	-1.64	-1.51	-1.29
4	-1.19	-1.42	-1.49	-1.46	-1.53	-1.22
5	-0.905	-1.19	-1.27	-0.874	-0.785	-0.511
6	-0.686	-0.75	-0.72	-0.634	-0.581	-0.358
7	-0.620	-0.555	-0.568	-0.502	-0.424	-0.280
8	-0.708	-0.489	-0.45	-0.393	-0.328	-0.249
9	-1.05	-0.45	-0.35	-0.262	-0.240	-0.249
10	-0.184	-0.096	-0.035	0.035	0.022	0.031
11	-0.118	-0.07	-0.018	0.044	0.061	0.079
12	-0.096	-0.052	0.009	0.087	0.101	0.118
13	-0.052	-0.009	-0.039	0.114	0.17	0.188
14	0.026	0.066	-0.087	0.197	0.262	0.284
15	0.153	0.284	-0.358	0.477	0.494	0.537
16	0.350	0.633	-0.525	0.634	0.59	0.720
17	0.669	0.847	0.865	0.830	0.918	0.925
C_c	0.005	-0.021	-0.219	-0.053	-0.055	-0.039
C_N	0.783	0.725	0.752	0.730	0.696	0.576
C_ℓ	0.733	0.688	0.714	0.704	0.674	0.553
C_d	0.273	0.228	0.236	0.200	0.187	0.160

DISTRIBUTION LIST FOR PROJECT REPORT NO. 57

of the St. Anthony Falls Hydraulic Laboratory

Copies	Organization
4	Office of Naval Research, Washington 25, D. C., Attn: [Code 438 (2), Code 461 (1), Code 465 (1)].
2	Commanding Officer, Office of Naval Research, Branch Office, John Crerar Library Building, 86 East Randolph Street, Chicago, Illinois.
1	Commanding Officer, Office of Naval Research, Branch Office, 346 Broadway, New York 13, New York.
1	Commanding Officer, Office of Naval Research, Branch Office, 1030 East Green Street, Pasadena 1, California.
1	Commanding Officer, Office of Naval Research, Branch Office, 1000 Geary Street, San Francisco, California.
25	Commanding Officer, Office of Naval Research, Navy #100, Fleet Post Office, New York, New York.
1	Chief of Naval Operations, Department of the Navy, Washington 25, D. C.
1	Director, Operations Research Office, Department of the Army, 7100 Connecticut Avenue, Chevy Chase, Maryland, Washington 15, D. C.
1	Office of the Secretary of Defense, The Pentagon, Washington 25, D. C., Attn: Weapons System, Evaluation Group.
1	Commandant, Marine Corps, Headquarters, U. S. Marine Corps, Washington 25, D. C., Attn: Asst. Chief of Staff, G-3.
1	Commandant, Marine Corps Schools, Quantico, Virginia, Attn: Director, Marine Corps, Development Center.
1	Assistant Chief of Transportation for Operations, Department of the Army, Bldg. T-7, Gravelly Point, Washington 25, D. C.
6	Director, Naval Research Laboratory, Washington 25, D. C., Attn: Code 2021.
2	Chief, Bureau of Aeronautics, Navy Department, Washington 25, D. C. Attn: [Code RS-1 (1), Code AD-314 (1)].
4	Chief, Bureau of Ordnance, Navy Department, Washington 25, D. C., Attn: [Code Re (1), Code ReO3 (1), Code ReU (1), Code ReU1-a (1)].
1	Commanding Officer, Naval Underwater Ordnance Station, Newport, Rhode Island.

Copies	Organization
7	Chief, Bureau of Ships, Navy Department, Washington 25, D. C., Attn: [Code 300 (1), Code 410 (1), Code 420 (1), Code 440 (1), Code 442 (1), Code 525 (1), Code 554 (1)].
1	Commander, Naval Ordnance Test Station, Inyokern, China Lake, California, Attn: Technical Library.
3	Commanding Officer and Director, David Taylor Model Basin, Washington 7, D. C., Attn: [Hydromechanics Lab (1), Seaworthiness & Fluid Dynamics Division (1), Library (1)].
1	Commanding Officer, Naval Ordnance Laboratory, White Oak, Maryland, Attn: Underwater Ordnance Department.
1	Director, Underwater Sound Laboratory, Fort Trumbull, New London, Connecticut.
1	Executive Secretary, Research & Development Board, Department of Defense, The Pentagon, Washington 25, D. C.
1	Chairman, Underseas Warfare Committee, National Research Council, 2101 Constitution Avenue, Washington 25, D. C.
1	Commanding General, Department of the Air Force, Washington 25, D. C., Attn: Director of Research and Development.
1	Director of Aeronautical Research, National Advisory Committee for Aeronautics, 1512 H Street, N. W., Washington 25, D. C.
2	Director, Langley Aeronautical Laboratory, National Advisory Committee for Aeronautics, Langley Field, Virginia, Attn: Mr. J. B. Parkinson.
1	Chief, Bureau of Yards and Docks, Navy Department, Washington 25, D. C., Attn: Research Division.
1	Commander, Naval Ordnance Test Station, 3202 East Foothill Boulevard, Pasadena, California, Attn: Head, Underwater Ordnance Dept.
1	Air Force Office of Scientific Research, Tempo T, Washington 25, D. C., Attn: Mechanics Division.
1	Librarian, U. S. Naval Postgraduate School, Monterey, California.
1	Dr. J. H. McMillen, National Science Foundation, 1520 H Street, N. W., Washington, D. C.
2	Director, National Bureau of Standards, Washington 25, D. C., Attn: Fluid Mechanics Section.
1	Gibbs and Cox, Inc., 21 West Street, New York 6, New York.

Copies	Organization
1	Dr. K. S. M. Davidson, Director, Experimental Towing Tank, Stevens Institute of Technology, 711 Hudson Street, Hoboken, New Jersey.
1	Mr. J. G. Baker, President, Baker Manufacturing Company, Evansville, Wisconsin.
1	Miami Shipbuilding Corporation, 615 S. W. Second Avenue, Miami 36, Florida.
1	Professor A. G. Strandhagen, Department of Engineering Mechanics, University of Notre Dame, Notre Dame, Indiana.
1	Hydrodynamics Research Laboratory, Consolidated-Vultee Aircraft Corporation, San Diego, California.
1	Douglas Aircraft Company, 3000 Ocean Park Boulevard, Santa Monica, California, Attn: Mr. A. E. Raymond.
1	Edo Corporation, College Point, Long Island, New York, Attn: Mr. W. R. Ryan.
1	The Grumman Aircraft Engineering Corporation, Calverton, Long Island, New York, Attn: Mr. Harvey Syndam.
1	The Martin Company, Baltimore 3, Maryland, Attn: Mr. J. D. Pierson.
1	Hughes Aircraft Company, Florence Avenue at Beal Street, Culver City, California.
1	Director, Waterways Experiment Station, Box 361, Vicksburg, Mississippi.
1	Beach Erosion Board, U. S. Army Corps of Engineers, Washington 25, D. C.
1	Director, Ballistics Research Laboratory, Department of the Army, Aberdeen Proving Ground, Aberdeen, Maryland.
1	Commissioner, Bureau of Reclamation, Washington 25, D. C.
1	Director, Oak Ridge National Laboratory, P. O. Box P, Oak Ridge, Tennessee.
1	Director, Applied Physics Division, Sandia Laboratory, Albuquerque, New Mexico.
5	Armed Services Technical Information Agency, Documents Service Center, Knott Building, Dayton 2, Ohio.
1	Office of Technical Services, Department of Commerce, Washington, D. C.

Copies	Organization
1	Brown University, Division of Applied Mathematics, Providence, Rhode Island, Attn: Dr. M. Holt.
4	University of California, Berkeley 4, California, Division of Mechanical Engineering, Attn: [Prof. H. A. Einstein (1), Prof. J. W. Johnson (1), Prof. H. A. Schade (1), Dr. J. V. Wehausen (1)].
1	Case Institute of Technology, Department of Mechanical Engineering, Cleveland, Ohio, Attn: Prof. G. Kuerti.
1	Cornell University, Graduate School of Aeronautical Engineering, Ithaca, New York, Attn: Prof. W. R. Sears, Director.
1	Harvard University, Department of Mathematics, Cambridge 38, Massachusetts, Attn: Prof. G. Birkhoff.
1	State University of Iowa, Iowa Institute of Hydraulic Research, Iowa City, Iowa, Attn: Dr. Hunter Rouse, Director.
1	Director, Applied Physics Laboratory, Johns Hopkins University, 8621 Georgia Avenue, Silver Spring, Maryland.
1	University of Maryland, Institute for Fluid Dynamics and Applied Mathematics, College Park, Maryland, Attn: Prof. M. H. Martin, Director.
2	Massachusetts Institute of Technology, Cambridge 39, Massachusetts, Attn: [Hydrodynamics Laboratory (1), Department of Naval Architecture (1)].
1	Michigan State College, Hydraulics Laboratory, East Lansing, Michigan, Attn: Prof. H. Henry.
1	University of Michigan, Applied Mechanics Department, Ann Arbor, Michigan, Attn: Prof. J. S. McNown.
1	New York University, Institute of Mathematical Science, 25 Waverly Place, New York 3, New York, Attn: Prof. R. Courant, Director.
1	University of Notre Dame, College of Engineering, Notre Dame, Indiana, Attn: Dean K. E. Schoenherr.
1	Pennsylvania State University, Ordnance Research Laboratory, University Park, Pennsylvania, Attn: Prof. G. F. Wislicenus.
2	Stanford University, Stanford, California, Attn: Applied Mathematics and Statistics Laboratory.
1	Worcester Polytechnic Institute, Alden Hydraulic Laboratory, Worcester, Massachusetts, Attn: Prof. J. L. Hooper, Director.

Copies	Organization
1	Aerojet General Corporation, 6352 North Irwindale Avenue, Azusa, California, Attn: Mr. C. A. Gongwer.
6	California Institute of Technology, Pasadena 4, California, Attn: Hydrodynamics Laboratory, [Library (1), Professor A. Hollander (1), Professor R. T. Knapp (1), Professor M. S. Plesset (1), Professor T. Y. Wu (1), GALCIT Professor C. B. Millikan, Director (1)].
1	University of Illinois, Department of Theoretical and Applied Mechanics, College of Engineering, Urbana, Illinois, Attn: Dr. J. M. Robertson.
1	Professor J. R. Weske, University of Maryland, Institute for Fluid Dynamics and Applied Mathematics, College Park, Maryland.
1	Prof. W. M. Rohsenow, Department of Mechanical Engineering, Massachusetts Institute of Technology, Cambridge 39, Massachusetts.
2	University of Michigan, Ann Arbor, Michigan, Attn: [Director, Engineering Research Institute (1), Professor V. L. Streeter, Civil Engineering Department (1)].
1	Rensselaer Polytechnic Institute, Department of Mathematics, Troy, New York, Attn: Dr. Hirsh Cohen.
1	Dr. Th. von Karman, 1051 South Marengo Street, Pasadena, California.